CELL BIOLOGY

Inhibition of IRF5 cellular activity with cell-penetrating peptides that target homodimerization

Jaspreet Banga[1]*, Dinesh Srinivasan[2]*†, Chia-Chi Sun[3], Cherrie D. Thompson[1], Francesca Milletti[4]‡, Kuo-Sen Huang[2], Shannon Hamilton[2], Su Song[1], Ann F. Hoffman[2]§, Yajuan Gu Qin[2], Bharati Matta[1], Margaret LaPan[1], Qin Guo[1], Gang Lu[2], Dan Li[1], Hong Qian[2]‖, David R. Bolin[2], Lena Liang[2], Charles Wartchow[2], Jin Qiu[3], Michelle Downing[3], Satwant Narula[2], Nader Fotouhi[2], Julie A. DeMartino[2,3], Seng-Lai Tan[2], Gang Chen[2,3]¶, Betsy J. Barnes[1,5]¶#

The transcription factor interferon regulatory factor 5 (IRF5) plays essential roles in pathogen-induced immunity downstream of Toll-, nucleotide-binding oligomerization domain–, and retinoic acid–inducible gene I–like receptors and is an autoimmune susceptibility gene. Normally, inactive in the cytoplasm, upon stimulation, IRF5 undergoes posttranslational modification(s), homodimerization, and nuclear translocation, where dimers mediate proinflammatory gene transcription. Here, we report the rational design of cell-penetrating peptides (CPPs) that disrupt IRF5 homodimerization. Biochemical and imaging analysis shows that IRF5-CPPs are cell permeable, noncytotoxic, and directly bind to endogenous IRF5. IRF5-CPPs were selective and afforded cell type– and species-specific inhibition. In plasmacytoid dendritic cells, inhibition of IRF5-mediated interferon-α production corresponded to a dose-dependent reduction in nuclear phosphorylated IRF5 [p(Ser^{462})IRF5], with no effect on pIRF5 levels. These data support that IRF5-CPPs function downstream of phosphorylation. Together, data support the utility of IRF5-CPPs as novel tools to probe IRF5 activation and function in disease.

INTRODUCTION

Interferon (IFN) regulatory factor 5 (IRF5) is a member of the IRF family of transcription factors. Similar to other family members, IRF5 was first identified as a transcriptional regulator of type I IFNs and IFN-stimulated genes in response to virus infection (*1*, *2*). Subsequent studies revealed important roles for IRF5 in innate and adaptive immunity, macrophage polarization, cell growth regulation, and apoptosis (*3*–*12*). Hence, dysregulation of IRF5 expression and/or function has been linked to the pathogenesis of numerous diseases, including autoimmune, infectious, cancer, obesity, neuropathic pain, cardiovascular, and metabolic dysfunction (*4*, *13*–*21*).

Through joint linkage and genome-wide association studies (GWASs), *IRF5* was identified as an autoimmune susceptibility gene (*22*). Polymorphisms in *IRF5* associate with risk of developing systemic lupus erythematosus (SLE), Sjögren's syndrome, and primary biliary cirrhosis (*23*–*28*). *IRF5* polymorphisms also associate with subgroups of patients with rheumatoid arthritis, antineutrophil cytoplasmic antibodies (ANCA) vasculitis, multiple sclerosis, and inflammatory bowel disease (*29*–*33*). Identification of *IRF5* as a susceptibility factor for these autoimmune disorders emphasizes the notion that similar immunogenetic mechanisms may underlie disease pathogenesis. IRF5 has been most studied in SLE, where its expression was found to be significantly elevated in peripheral blood mononuclear cells (PBMCs) from patients with SLE as compared with healthy donors (*34*). Stratification of patients with SLE by risk polymorphisms revealed that homozygous risk carriers had elevated IRF5 expression and type I IFN activity (*34*, *35*). Data from GWASs have now been complemented by mouse and preclinical human studies, suggesting that IRF5 may promote autoimmunity through several mechanisms and pathways (*34*–*43*). Results from mouse models of lupus showing protection from disease onset and severity in mice lacking *Irf5* support a pathogenic role for IRF5 in SLE and the rational targeting of IRF5 inhibition (*36*, *39*–*42*, *44*). Murine studies revealed a crucial role for Irf5 in Toll-like receptor (TLR)–dependent proinflammatory cytokine expression [IFNα, interleukin-12 (IL12), tumor necrosis factor–α (TNFα), and IL6], pathogenic autoantibody production, and T helper 1 (T_H1) immune response(s) (*34*, *36*, *45*). In SLE monocytes, IRF5 activation was found to be significantly elevated, as determined by its nuclear localization when compared with healthy donors (*37*). Other studies implicated IRF5 as a master switch that promotes proinflammatory cytokine production from dendritic cells and macrophages and thus contributes to the plasticity of macrophage polarization (*11*, *46*). More recently, data show that IRF5 plays an important role in TLR9/B cell receptor–induced plasmablast differentiation and antibody secretion (*12*, *47*). Collectively, these findings provide a compelling rationale for the development of therapeutic agents targeting IRF5 for the treatment of SLE and other autoimmune diseases.

Thus far, preclinical studies have relied entirely on the use of small interfering RNA targeting *IRF5* or *Irf5*$^{-/-}$ mice; however, there are limitations to interpreting data from either of these approaches (*12*, *47*). The availability of a specific tool(s) that can mimic the consequences

[1]The Feinstein Institute for Medical Research, Center for Autoimmune, Musculoskeletal and Hematopoietic Diseases, 350 Community Dr., Manhasset, NY 110301, USA. [2]Hoffmann-La Roche Inc., 340 Kingsland Street, Nutley, NJ 07110, USA. [3]EMD Serono Research and Development Institute Inc., 45A Middlesex Turnpike, Billerica, MA 01821, USA. [4]Roche Innovation Center New York, 430 East 29th Street, New York, NY 10016, USA. [5]Departments of Molecular Medicine and Pediatrics, Zucker School of Medicine at Hofstra/Northwell, Hempstead, NY 11549, USA.
*These authors contributed equally to this work.
†Present address: AzurRx BioPharma Inc., 760 Parkside Avenue, Downstate Biotechnology Incubator, Suite 304, Brooklyn, NY 11226, USA.
‡Present address: Kite Pharma, 1800 Stewart Street, Santa Monica, CA 90404, USA.
§Present address: Platform of Technology and Science, GlaxoSmithKline, 1250 S Collegeville Rd., Collegeville, PA 19426, USA.
‖Present address: Novartis Pharmaceuticals, 1 Health Plaza, East Hanover, NJ 07936, USA.
¶Corresponding author. Email: bbarnes1@northwell.edu (B.J.B.); gang.chen@emdserono.com (G.C.)
#Lead contact.

associated with pharmacological inhibition of IRF5 in human cells would greatly advance our understanding of IRF5 function. Structure-function data and partial resolution of the C-terminal crystal structure of IRF5 have offered key insights into the molecular steps required for IRF5 activation, suggesting that IRF5 dimerization may be an essential step for nuclear translocation and downstream signaling (*48*). Here, we designed antagonistic cell-penetrating peptides (CPPs) by incorporating the native amino acid sequence of IRF5 to directly interrogate the mechanism(s) of IRF5 activation and function in human primary immune cells.

RESULTS

Identification of novel CPP motifs and design of CPPs targeting IRF5

Visual inspection of the dimeric IRF5 crystal structure (Fig. 1A) revealed the importance of interactions between Helix 2 and Helix 5 of different IRF5 monomers for dimerization. These large interaction sites are likely intractable to intervention with small molecules, but we hypothesized that they might be amenable to peptide antagonists. Using computational methods that we recently described for the identification of short hydrophobic CPPs (*49*), we analyzed scaled polarity (PP1) and hydrophobicity (PP2) scores that reflect the interaction of individual amino acid residues with different chemical moieties, to predict CPP functionality. From the test dataset shown in Fig. 1B, 109 CPP sequences and 1000 non-CPP (decoy) sequences were categorized using this scoring method (*49*); less than 1% of decoy sequences were found in the green region corresponding to good cell penetration scores. On the basis of this analysis, two CPP templates, mouse prion protein (mPrP; amino acids 1 to 28) and YLKFIPLKRAIWLIK (YLK) (Fig. 1B), were selected for conjugation with IRF5 sequences. Putative IRF5-CPPs were generated by either conjugating the CPP sequence directly to an IRF5 Helix 2 or Helix 5 sequence, using a connector sequence for conjugation, or by interweaving residues at the interface of Helix 2 and Helix 5 from IRF5 with CPP sequences (see Materials and Methods, Table 1, and fig. S1). Thirty-eight peptides were synthesized using the YLK sequence from *Saccharomyces cerevisiae* mediator of RNA polymerase II transcription subunit 12 (amino acids 161 to 176) or the MANLGYWLLALFVTMWTDVGLCKKRPKP motif from mPrP to confer cell penetration of selected IRF5 amino acid sequences (Helix 2, Helix 5, or connector). Peptides were screened by biochemical and cellular assays to determine their ability to enter the cell and interact with IRF5.

IRF5-CPPs interact with recombinant and intracellular IRF5 to inhibit homodimerization

Fluorescein isothiocyanate (FITC)–labeled versions of IRF5-CPPs were tested in a direct binding assay. His-tagged IRF5, consisting of amino acids 222 to 425 to minimize dimerization (*48*), was used to determine whether FITC-IRF5-CPPs could bind to the monomeric form of IRF5. Six (IRF5-CPPs 1 to 6) of the 38 FITC-labeled peptides tested bound IRF5 with submicromolar dissociation constant (K_d) (Fig. 1C and Table 1); FITC-CPP7 served as a negative control peptide since it contained only the YLK CPP sequence and no IRF5-specific sequence. Unlabeled IRF5-CPPs 1 to 6 were also confirmed to directly bind to IRF5 using a thermal shift assay, albeit with small degrees of change (table S1). Since the SD of IRF5 alone with no CPP was 0.1°C, a melting temperature (T_m) greater than three times the SD was considered a binder to IRF5 (>0.3°C), although the thermal shift itself was generally less than 2°C for each IRF5-CPP. For the identification of IRF5-CPPs that inhibit IRF5 homodimerization, a time-resolved fluorescence resonance energy transfer (TR-FRET)–based biochemical assay was developed (*50*). Full-length IRF5 was tagged with either His or biotin at the C terminus and TR-FRET performed. His-tagged wild-type (WT) IRF5 and biotin-tagged WT IRF5 homodimerized with an estimated K_d of 4.21 ± 0.06 μM. Previously, Chen *et al.* (*48*) reported that the amino acid substitution S430D, which was introduced to mimic constitutive phosphorylation of IRF5 at this critical residue, favored dimerization in solution and promoted transcriptional activation. In accordance with their work, we found that the S430D monomers had a ~7-fold higher affinity (K_d = 0.60 ± 0.05 μM) for dimerization as compared to WT monomers. When the S430D and WT monomers were tested together, an intermediate affinity was observed (K_d = 1.58 ± 0.22 μM). Using this assay, we determined the ability of IRF5-CPPs to inhibit IRF5 homodimerization. Among the 38 peptides tested, IRF5-CPPs 2 to 6 inhibited dimerization of S430D and WT in a concentration-dependent manner with potencies listed in table S2. All other peptides tested had potencies of >75 μM. Notably, FITC-conjugated IRF5-CPPs showed increased ability to inhibit IRF5 homodimerization, albeit the trend in inhibition was identical between nonconjugated and FITC-conjugated peptides. While FITC itself does not interfere with this assay, addition of FITC to the N terminus of IRF5-CPPs may provide additional hydrophobic interactions.

We next performed Native gel electrophoresis on THP-1 cells stimulated with R848 to further confirm the effect of IRF5-CPPs on IRF5 homodimerization. THP-1 monocytes express high levels of endogenous IRF5 and respond to the TLR7 ligand R848 to induce IRF5 nuclear translocation (*6*). We examined the ability of IRF5-CPP2 and IRF5-CPP5 to inhibit TLR7-induced IRF5 homodimerization as they provided the lowest median inhibitory concentration (IC_{50}) values by biochemical assay (Fig. 1C and table S2) and represent two distinct methods of targeting dimerization (Table 1). THP-1 cells were preincubated with 1 and 10 μM IRF5-CPPs for 1 hour, followed by stimulation with 1 μM R848 for 1 hour (*6*). As expected, an increase in endogenous IRF5 homodimerization after 1-hour stimulation was detected (Fig. 1, D and F). While little effect of IRF5-CPP2 on IRF5 homodimerization was seen, a dose-dependent decrease in R848-induced homodimerization by IRF5-CPP5 was found (Fig. 1, E and F, and fig. S2, A and B). Given that family members IRF3 and IRF7 also undergo dimerization in response to TLR stimulation (*44*, *51*), we used this assay to assess specificity of IRF5-CPP2 and IRF5-CPP5 for IRF5 by analyzing IRF3 and IRF7 homodimerization under the same conditions. Expectedly, we detected only low levels of IRF3 homodimerization in response to R848 stimulation (*52*), which were not affected by IRF5-CPP2 or IRF5-CPP5. While the levels of IRF7 homodimerization were increased after R848 stimulation, they were also unaffected by IRF5-CPPs (fig. S1, C and D). To further confirm specificity of IRF5-CPP2 and IRF5-CPP5 for IRF5, we synthesized two negative control peptides: IRF5-CPP8 is a scrambled version of IRF5-CPP2, and IRF5-CPP9 is identical to IRF5-CPP5 but lacks the IRF5-specific sequences (Table 1). Neither of these two peptides inhibited intracellular IRF5 homodimerization at 10 μM, which is the concentration we detected the strongest inhibition by IRF5-CPP5 (Fig. 1, D to F).

We then developed an intracellular FRET (in-cell FRET) assay (*53*) to measure the interaction of FITC-conjugated IRF5-CPPs with

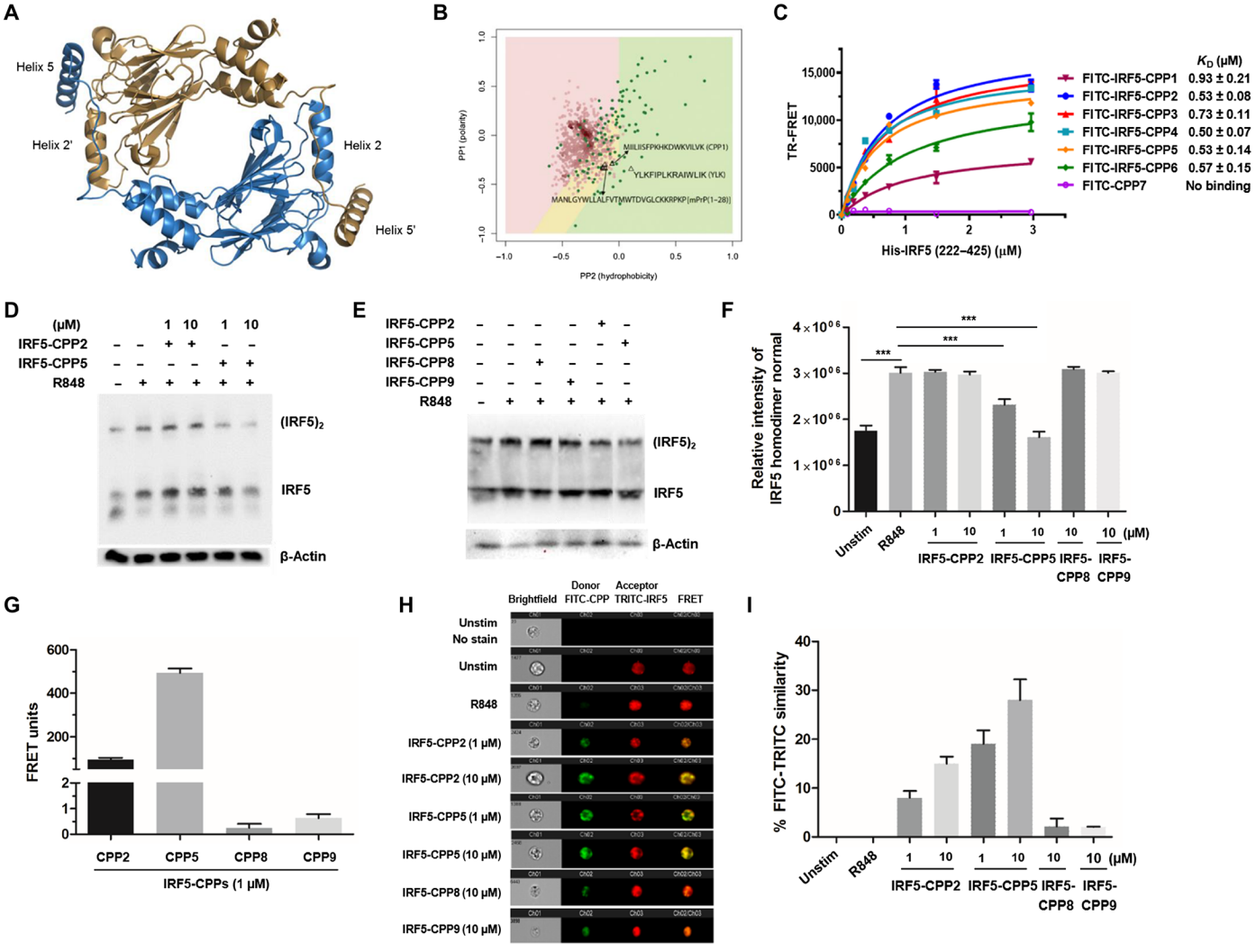

Fig. 1. Binding of IRF5-CPPs to IRF5. (**A**) The crystal structure of dimeric IRF5 highlights the importance of interactions between Helix 2 and Helix 5 of different monomers for dimerization. One monomer is shown in blue, and the other is shown in brown. (**B**) Polarity and hydrophobicity plot of CPPs. Two CPP templates, mPrP (*1–28*) and YLK, were selected for testing with IRF5 sequences. Green- and yellow-shaded regions denote good to moderate cell penetration, respectively, while pink denotes no penetration. (**C**) Individual curves generated from time-resolved fluorescence resonance energy transfer (TR-FRET) using fluorescein isothiocyanate (FITC)–labeled IRF5-CPPs, the YLK CPP control FITC-CPP7 and His-tagged IRF5. All six IRF5-CPP peptides bound to IRF5 (222 to 425) with submicromolar potencies, while the negative YLK CPP control did not. (**D**) Representative Native gel electrophoresis showing effect of IRF5-CPP2 and IRF5-CPP5 on R848-induced IRF5 homodimerization in THP-1 cells. Stimulation with 1 μM R848 for 1 hour induced intracellular IRF5 homodimerization (lane 2). Preincubation with IRF5-CPP5 provided a dose-dependent reduction in R848-induced IRF5 homodimerization. (**E**) Same as (D) except scrambled negative control IRF5-CPP8 and IRF5-CPP9 were examined by cellular IRF5 homodimerization assay. (**F**) Quantification of IRF5 homodimerization from (D) and (E) is shown after normalization to β-actin. One-way analysis of variance (ANOVA) with Bonferroni's multiple comparison test was performed. ***$P < 0.001$, ****$P < 0.0001$. (**G**) THP-1 cells were preincubated with FITC-CPP2, FITC-CPP5, FITC-CPP8, or FITC-CPP9 for 1 hour, followed by permeabilization and staining for intracellular IRF5 with tetramethyl rhodamine isothiocyanate (TRITC)–conjugated antibodies. FRET units were calculated from fluorescence emissions (see Materials and Methods). (**H**) Representative cellular images of in-cell FRET from 10,000 acquired events by imaging flow cytometry is shown. (**I**) Percentage of THP-1 cells from (H) showing FRET signal by FITC-TRITC similarity score. Data in (D) to (I) are representative of three independent experiments performed in triplicate with SD shown in (F), (G), and (I).

endogenous IRF5. THP-1 cells were preincubated with 1 μM FITC-IRF5-CPPs for 1 hour, followed by staining with tetramethyl rhodamine isothiocyanate (TRITC)–IRF5 antibodies. While both FITC-IRF5-CPP2 and FITC-IRF5-CPP5 were found to emit a FRET signal, supporting close interaction (<10 nm) of each with TRITC-IRF5, the FITC-TRITC emission signal by IRF5-CPP5 and IRF5 was ~4-fold greater than IRF5-CPP2 and IRF5 (Fig. 1G). Notably, IRF5-CPP8 and -CPP9 showed minimal FRET signal, confirming their inability to bind to intracellular IRF5. Representative images and quantification from imaging flow cytometry (*54*, *55*) of FITC-IRF5-CPPs and TRITC-IRF5 confirmed the differential FRET emission signal by these four IRF5-CPPs (Fig. 1, H and I). Together, these data confirm that while both IRF5-CPP2 and IRF5-CPP5 directly interact with recombinant and endogenous IRF5, a stronger FRET emission signal was detected

Table 1. Inhibitor sequences with the type of CPP used.

CPP #	Sequence*†	Type
IRF5-CPP1	Ac-IRLQISNPYLKFIPLKRAIWLIK-NH_2	Connector + CPP
IRF5-CPP2	Ac-MIILIISFPKHKDWKVILVK-NH_2	Helix 5 + Connector interwoven
IRF5-CPP3	MANLGYWLLLLFVTMWTDVGLAKKRPKP	Helix 2 interwoven
IRF5-CPP4	MANLGYWLALLFVTMWTDVGLFKKRPKP	Helix 2 interwoven
IRF5-CPP5	MANLGYWLLALFVTYWTDLGLVKKRPKP	Helix 2 interwoven
IRF5-CPP6	MANLGYWLYALFLTMVTDVGLFKKRPKP	Helix 2 interwoven
CPP7	Ac-YLKFIPLKRAIWLIK-NH_2	YLK CPP control
IRF5-CPP8	Ac-IKVMWPILFIIKLVHSDKKI-NH_2	Scrambled IRF5-CPP2
IRF5-CPP9	MANLGYWLLALFVTMWTDVGLCKKRPKP	Negative control for IRF5-CPP5

*IRF5-derived amino acid residue should show up in "red" font. †Non-IRF5 residues should show up in green.

with FITC-IRF5-CPP5 and TRITC-IRF5, resulting in the dose-dependent inhibition of R848-induced IRF5 homodimerization.

IRF5-CPPs are noncytotoxic and cell penetrant

Cytotoxicity of IRF5-CPPs 1 to 6 was examined by CellTiter-Glo assay in HeLa cells; all six peptides were found to be noncytotoxic up to 50 μM (fig. S3). The ability of IRF5-CPPs to penetrate a cell and colocalize with endogenous IRF5 was examined by imaging flow cytometry in human primary immune cells. PBMCs from healthy donors were isolated and incubated with 5 μM FITC-IRF5-CPPs for 30 and 60 min. Cells were surface-stained, fixed, and permeabilized for intracellular IRF5 staining (*37*). IRF5-CPP internalization and colocalization with endogenous IRF5 were examined in $CD19^+$ B cells, $CD14^+$ monocytes, and $BDCA2^+CD123^+$ plasmacytoid dendritic cells (pDCs), as these are relevant cell types for examining IRF5 biologic function. Figure 2A shows representative data from imaging flow cytometry of B cells after 30- and 60-min incubation of PBMCs with FITC-IRF5-CPP5. At 30-min incubation, 50.3% of $CD19^+$ B cells had FITC-labeled peptides on the external cell surface (Fig. 2A, left, quadrant A), 30.5% had internalized peptides (Fig. 2A, left, quadrant B), and 19.2% had internalized and colocalized CPP5 with endogenous IRF5 (Fig. 2A, left, quadrant C). After 60-min incubation with FITC-IRF5-CPP5, peptide internalization was significantly enhanced, and colocalization of FITC-IRF5-CPP5 with endogenous IRF5 occurred in the cytoplasm of B cells (Fig. 2B). Cellular images from each quadrant in Fig. 2A are shown in Fig. 2B; data from B cells is summarized in Fig. 2C. In all three cell types, significant internalization of FITC-IRF5-CPP2 and FITC-IRF5-CPP5 at 5 μM was detected, along with FITC-IRF5-CPP and IRF5 colocalization (Fig. 2, B to G).

Inhibition of TLR7/8-dependent proinflammatory cytokine production and IRF5 nuclear translocation by IRF5-CPPs

IRF5 is a critical downstream mediator of myeloid differentiation primary response protein (MyD88)–dependent TLR signaling (*5*, *6*), and TLR7/8/9 have been implicated in the pathogenesis of SLE. To determine whether internalized and colocalized IRF5-CPPs were functionally active, we examined their ability to attenuate R848-induced proinflammatory cytokine production. Healthy donor PBMCs were pretreated with various concentrations of IRF5-CPPs (or vehicle) for 30 min before stimulation with 1 μM R848 overnight. Results show that all six IRF5-CPPs were able to inhibit IL12p40 production with varying potencies (Fig. 3A). IRF5-CPP2 and IRF5-CPP5 were brought forward for further analysis of their effects on R848-induced IRF5 nuclear translocation (activation) since they gave the most potent inhibition of cytokine production (>50% inhibition at 5.56 μM). IRF5 nuclear translocation was measured by imaging flow cytometry at 2 hours after stimulation in $CD14^+$ monocytes and $CD19^+$ B cells. Gating strategy is shown in fig. S4A.In both cell types, R848 induced ~3-fold increase in IRF5 nuclear accumulation as compared with vehicle-stimulated (Fig. 3, B and C). In monocytes, both CPPs provided concentration-dependent inhibition from 0.6 to 5.56 μM, but at 16 μM, the inhibitory effect was lost (Fig. 3B). Conversely, in B cells, concentration-dependent inhibition occurred over the range (Fig. 3C). Representative images of R848-induced IRF5 activation and inhibition by IRF5-CPP2 and IRF5-CPP5 are shown (Fig. 3D). The ability of IRF5-CPP8 and IRF5-CPP9 to inhibit R848-induced IRF5 nuclear translocation was also examined; neither peptide provided IRF5-specific inhibition in $CD14^+$ monocytes or $CD19^+$ B cells (fig. S4, B and C). Last, findings from imaging flow cytometry were confirmed by Western blot analysis of cyto/nuclear extracts from human primary monocytes preincubated with a dose response of IRF5-CPP2 or IRF5-CPP5 for 30 min before stimulation with R848 for 2 hours (fig. S5, A and B).

Inhibition of IRF5-mediated macrophage function by IRF5-CPPs

IRF5 also plays important roles in macrophage function, including the regulation of macrophage polarization, differentiation, and cytokine expression (*11*, *56*–*58*). We thus generated human primary monocyte-derived macrophages (MDMs) to test the effect of IRF5-CPP2 and -CPP5 on lipopolysaccharide (LPS)– or R848-induced cytokine production. We detected a significant reduction in LPS-induced cytokine production from IRF5-CPP5, but not IRF5-CPP2-treated MDMs, at both the transcript and protein levels (Fig. 4, A to F, and fig. S6, A to H). Notably, significant inhibition of cytokine expression/production by IRF5-CPP5 was detected equally across all doses examined (Fig. 4, A to F). While R848 was not as strong an inducer of cytokines as LPS in MDMs, a similar inhibitory profile was detected for IRF5-CPP5 at both the transcript and protein levels. We also examined IRF5-CPP2 and IRF5-CPP5 effects

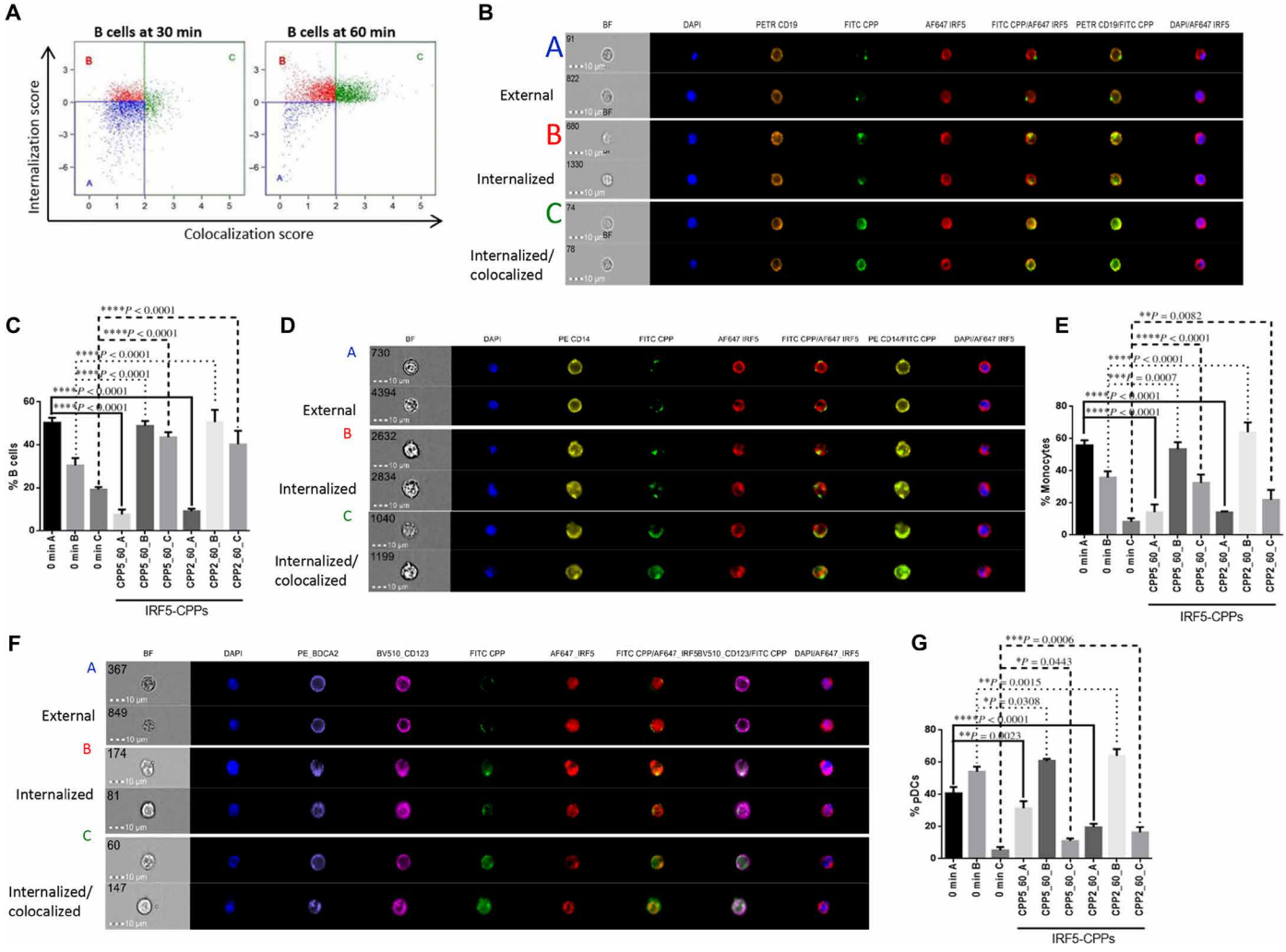

Fig. 2. IRF5-CPPs are cell penetrant and colocalize with endogenous IRF5. (**A**) Representative dot plots from imaging flow cytometry of gated CD19$^+$ B cells from PBMCs showing differential internalization and colocalization of FITC-IRF5-CPP5 with endogenous IRF5. FITC-CPP5 (1 μM) was incubated with PBMCs for 30 or 60 min. Quadrant A (bottom left) shows CD19$^+$ B cells that have not internalized FITC-IRF5-CPP5, and FITC-IRF5-CPP5 is not localized with IRF5. Quadrant B shows CD19$^+$ B cells that have internalized FITC-IRF5-CPP5, but FITC-IRF5-CPP5 is not colocalized with IRF5. Quadrant C shows CD19$^+$ B cells that have both internalized and colocalized FITC-IRF5-CPP5 with IRF5. (**B**) Representative cellular images from each quadrant in (A). DAPI, 4′,6-diamidino-2-phenylindole; BF, brightfield; PETR, Texas red. (**C**) Summarized data of 1 μM FITC-IRF5-CPP2 and FITC-IRF5-CPP5 internalization and IRF5 colocalization from gated CD19$^+$ B cells. (**D** and **E**) Representative images are shown for CD14$^+$ monocytes (D) along with summarized data (E). (**F** and **G**) Representative images and summarized data for BDCA2$^+$CD123$^+$ pDCs are shown. Data are from three independent healthy donors; reported errors indicate SD. One-way ANOVA with Bonferroni's multiple comparison test was performed.

on murine bone marrow–derived macrophages (BMDMs) stimulated with LPS or R848. Somewhat unexpected, we found the opposite effect in murine BMDMs with only IRF5-CPP2 showing select inhibition of murine Irf5-mediated cytokine production in WT and not *Irf5*$^{-/-}$ BMDMs (Fig. 4, G to I, and fig. S6I). Significant inhibition was only found at the highest dose of 15 μM (Fig. 4, G to I). While IRF5-CPP2 had no significant effect on LPS- or R848-induced cytokine production in *Irf5*$^{-/-}$ BMDMs, consistent with previous reports, *Irf5*$^{-/-}$ BMDMs are already deficient in their ability to secrete these cytokines (*5*, *11*, *56*). Thus, in efforts to further ascertain IRF5-CPP2 specificity, we examined additional cytokines, such as transforming growth factor β (TGFβ), that were up-regulated after stimulation but unaffected by loss of *Irf5* or treatment with IRF5-CPP2 (fig. S6I). Together, data support the specificity of IRF5-CPP2 and IRF5-CPP5 for IRF5 and indicate that they have distinct species-specific effects in human MDMs and murine BMDMs.

IRF5-CPPs inhibit TLR9-mediated effects in primary B cells and pDCs

Studies in *Irf5*$^{-/-}$ mice, lymphoblastoid cell lines from patients with SLE, and human primary naïve B cells indicate an important role for IRF5 in B cell effector function (*12*, *36*, *40*, *59*). Data from murine models of SLE show that *Irf5*$^{-/-}$ mice are protected from pathogenic immunoglobulin G (IgG) production (*36*, *39*–*42*, *45*). To determine whether a similar function(s) exists in human cells, CD19$^+$ B cells were isolated from healthy donors, incubated with IRF5-CPPs, and stimulated with CpGB [ODN(oligonucleotides)2006] plus IL2 for 7 days to induce IgG production. Data in Fig. 5A reveal

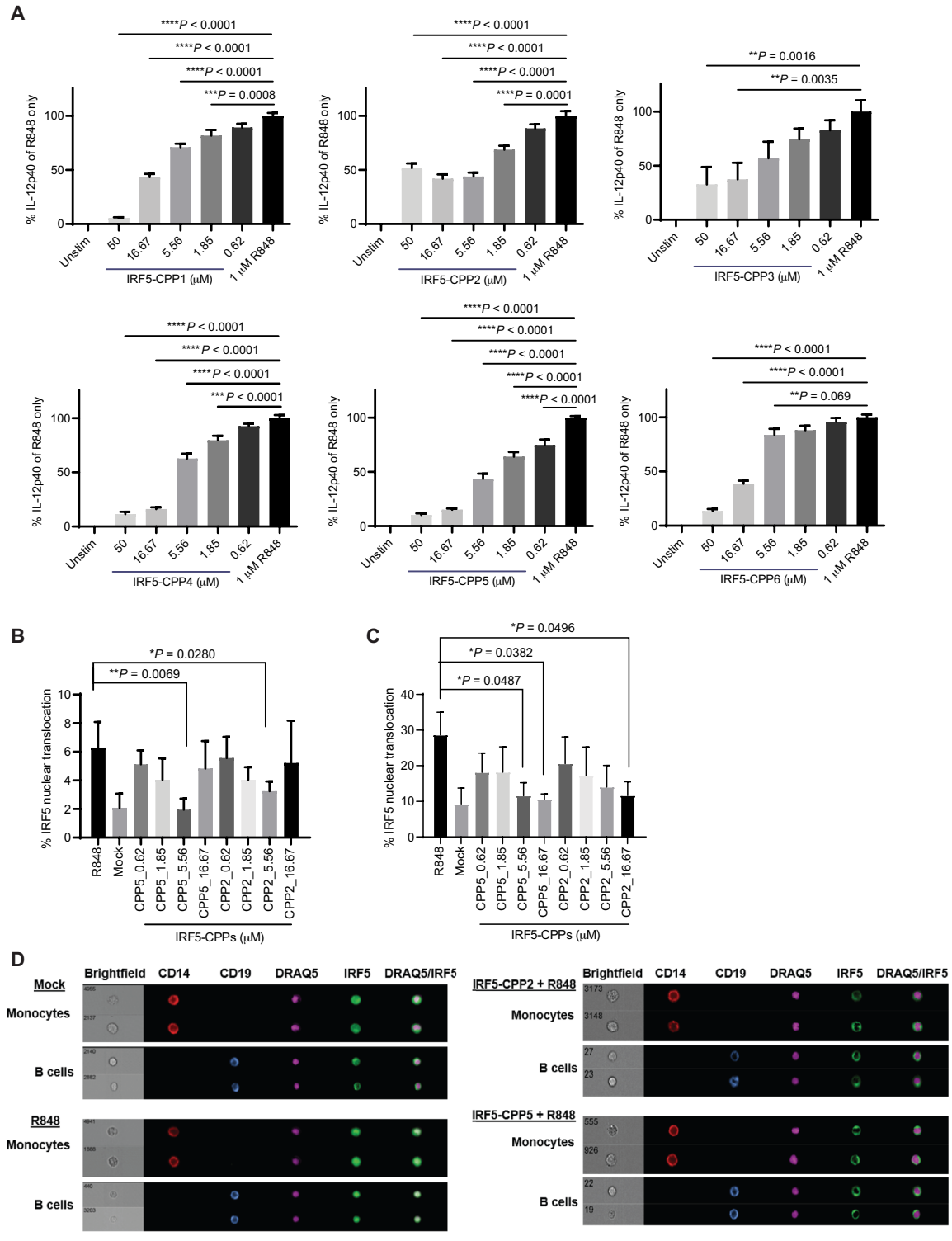

Fig. 3. IRF5-CPPs inhibit IL12 production from human PBMCs and IRF5 nuclear translocation in a concentration-dependent manner. (**A**) Human PBMCs were pretreated for 30 min with various concentrations of IRF5-CPPs and stimulated overnight with 1 μM R848. IL12p40 levels in supernatant were measured by enzyme-linked immunosorbent assay (ELISA) and normalized to values from wells stimulated with 1 μM R848 and peptide vehicle [0.05% dimethyl sulfoxide (DMSO) and 5% water]. Summarized data are from $n = 4$ healthy donors performed in triplicate; reported errors indicate SEM. Percentage of $CD14^+$ monocytes (**B**) and $CD19^+$ B cells (**C**) with nuclear-localized IRF5. PBMCs were preincubated with the indicated concentrations of IRF5-CPP2 or IRF5-CPP5, stimulated with 1 μM R848 for 2 hours, stained for IRF5 and nuclear DRAQ5 (deep red anthraquinone 5), and then subjected to imaging flow cytometry. Nuclear translocation was defined as cells with a similarity score of IRF5 and DRAQ5 of ≥1.5. Data are from $n = 4$ independent donors; reported errors indicate SD. (**D**) Representative images of $CD19^+$ B cells and $CD14^+$ monocytes from (B) and (C). One-way ANOVA with Bonferroni's multiple comparison test was performed.

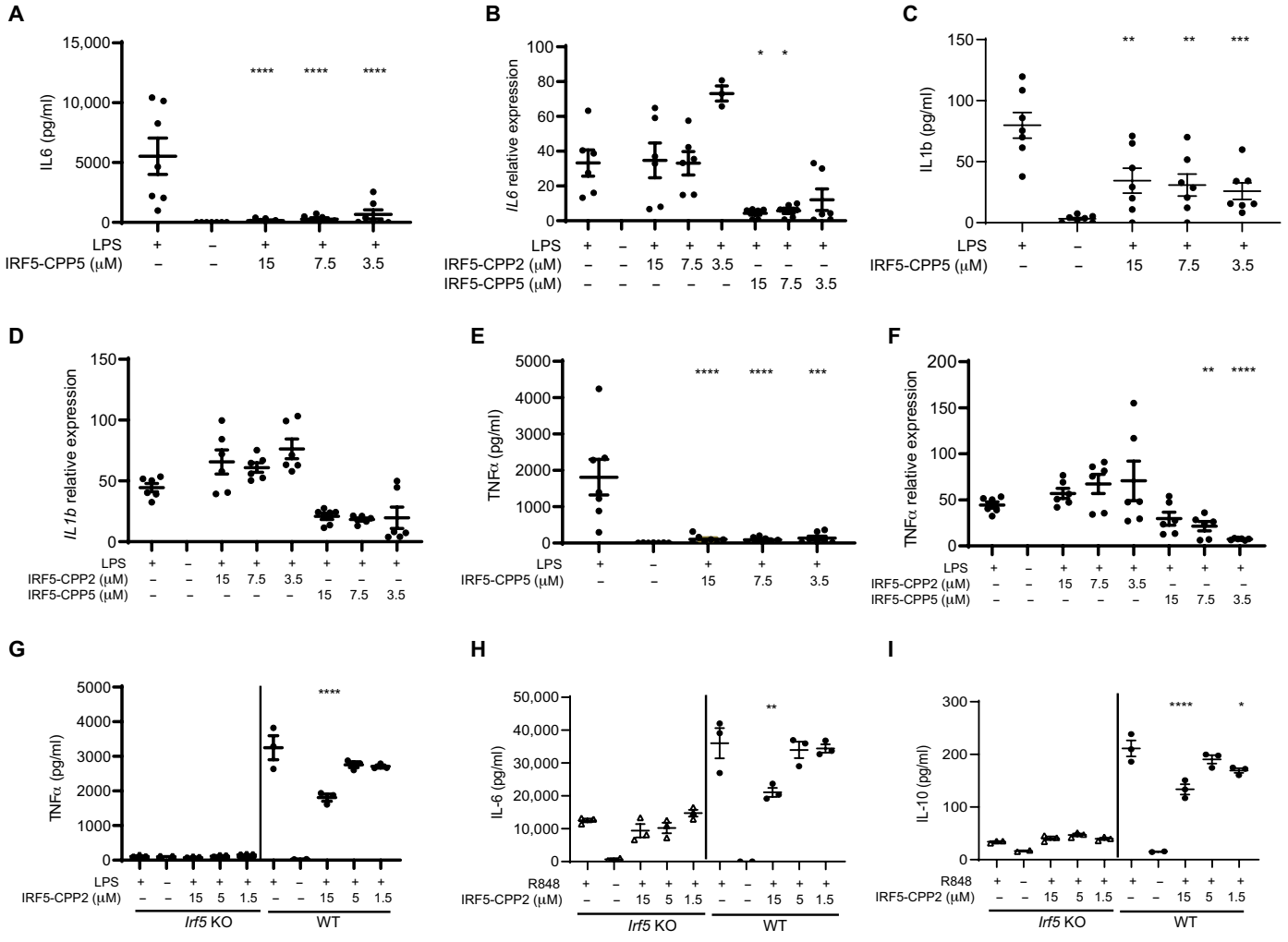

Fig. 4. Species-specific inhibition of macrophage-mediated cytokine expression by IRF5-CPP2 and IRF5-CPP5. (**A** to **F**) Human MDMs were pretreated for 1 hour with various concentrations of IRF5-CPP2 and IRF5-CPP5 and stimulated with LPS for 4 hours to assess transcript expression by quantitative polymerase chain reaction (qPCR) and 24 hours to assess cytokine production by ELISA. Summarized data are from $n = 6$ to 7 healthy donors performed in triplicate; reported errors indicate SEM. (**G** to **I**) BMDMs from *Irf5*$^{-/-}$ and littermate-matched WT mice were pretreated with IRF5-CPP2 and stimulated with LPS for 24 hours for analysis of cytokine production in cell supernatants. KO, knockout. Data shown are from $n = 3$ mice per genotype and performed in triplicate. Statistical analysis performed between LPS- or R848-stimulated, nontreated, and IRF5-CPP–treated cells. One-way ANOVA with Bonferroni's multiple comparison test was performed. *$P \leq 0.05$, **$P \leq 0.005$, ***$P \leq 0.0005$, and ****$P < 0.0001$.

that most IRF5-CPPs attenuated IgG production at a concentration of >2.78 μM. IRF5-CPP1 and IRF5-CPP2 were the most potent, providing ≥50% inhibition of total IgG production at 2.78 μM. Similar to Fig. 3 (B and C), IRF5-CPP2 and IRF5-CPP5 provided concentration-dependent inhibition of IRF5 nuclear translocation in B cells at 2 hours after stimulation (Fig. 5B).

A key cytokine implicated in SLE pathogenesis is IFNα. Approximately 50% of patients with SLE carry an IFN gene signature, and the *IRF5*-SLE–risk haplotype significantly associates with elevated IFN activity (*35*). Since pDCs are the primary producers of IFNα, we analyzed the effect of IRF5-CPPs on CpGA-induced IFNα secretion. Healthy donor pDCs were isolated and stimulated overnight with CpGA (ODN2216; 1 μM), and IFNα levels were measured by enzyme-linked immunosorbent assay (ELISA). All IRF5-CPPs blocked IFNα production in a concentration-dependent manner with varying potencies (Fig. 5C). IRF5-CPP2 was the most potent and even highly active at the lowest concentration (0.62 μM). Somewhat unexpected, inhibition of IFNα production at this low concentration did not correlate with a concomitant reduction in CpGA-induced IRF5 activation (Fig. 5D). Data, instead, suggested that IRF5-CPP2 may be targeting IRF7 activation (*51*). Although we saw no change in TLR7-induced IRF7 homodimerization by IRF5-CPP2 in monocytes (fig. S2D), we examined the effect of IRF5-CPP2 on CpGA-induced IRF7 nuclear translocation in pDCs by imaging flow cytometry. We were unable to detect a significant change in IRF7 nuclear translocation over a dose response of IRF5-CPP2 (fig. S7A). We then extended our analysis to nuclear factor κB (NF-κB) since IRF5 and NF-κB regulate similar target genes in myeloid cells (*60*, *61*). First, IRF5-CPPs were tested in a TNFα-induced RelA (p65 subunit of NF-κB) nuclear translocation assay, revealing minimal effects on NF-κB nuclear translocation at a concentration of ≤50 μM (fig. S7B). Second, by imaging flow cytometry, we confirmed that IRF5-CPP2 and IRF5-CPP5 have no significant effect on TLR-induced NF-κB nuclear translocation (fig. S7C). Last, by in-cell FRET, we confirmed that IRF5-CPP2

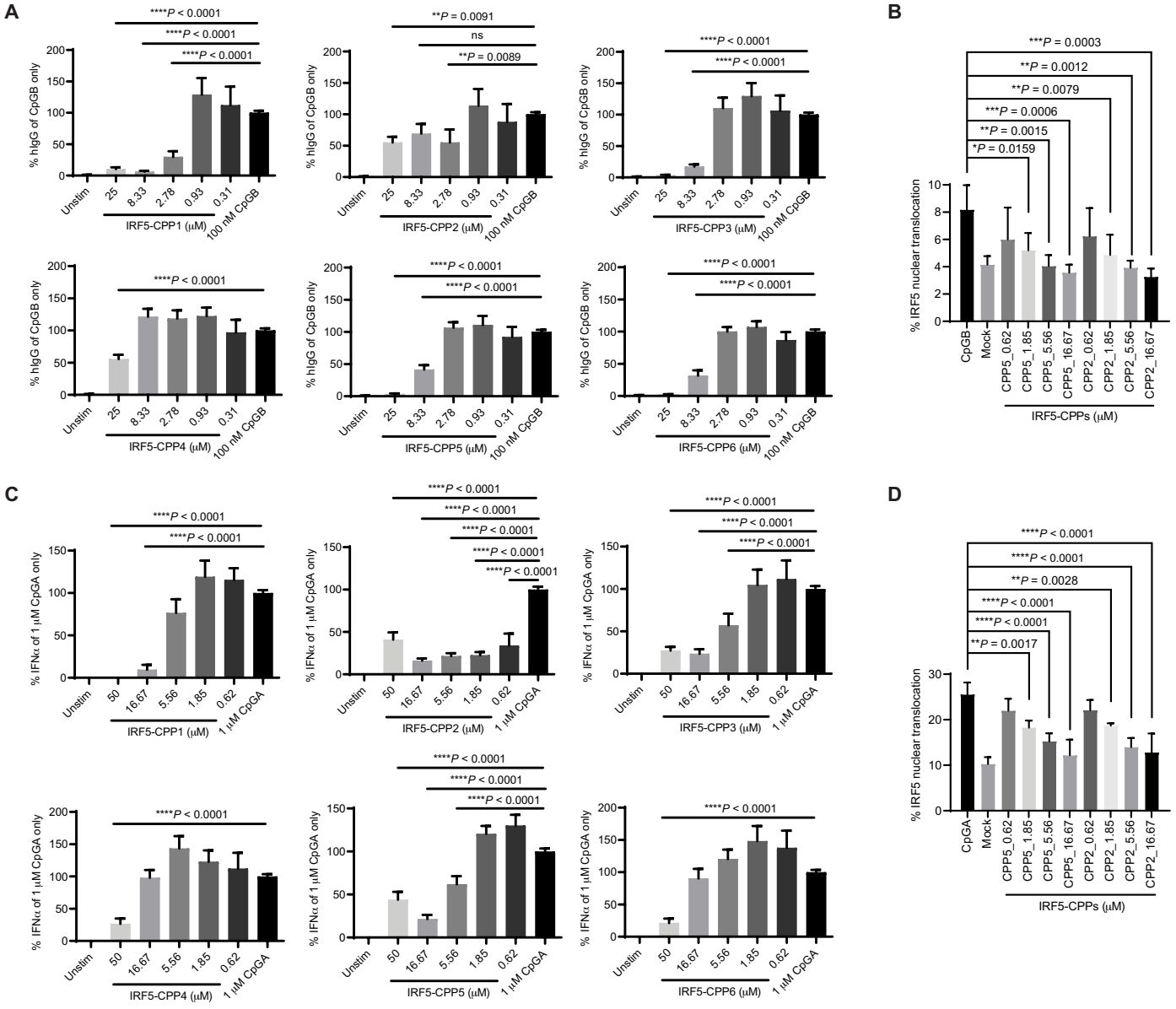

Fig. 5. IRF5-CPPs attenuate IgG production from human B cells and type I IFN production from human pDCs through inhibition of IRF5 nuclear translocation. (**A**) Freshly isolated B cells were pretreated for 30 min with various concentrations of IRF5-CPPs and stimulated for 7 days with 100 nM CpGB. IgG levels in supernatant were measured by AlphaLISA and normalized to values obtained from wells stimulated with 100 nM CpGB and peptide vehicle. Graphs represent data from $n = 3$ healthy donors measured in triplicate; error bars indicate SEM. ns, not significant. (**B**) PBMCs were pretreated with IRF5-CPP2 or IRF5-CPP5 and stimulated with CpGB for 2 hours. The percentage of $CD19^+$ B cells with nuclear-localized IRF5 is shown with SD. (**C**) Same as (A) except freshly isolated pDCs were pretreated with IRF5-CPPs and stimulated ON (overnight) with 1 μM CpGA. IFNα levels in supernatant were measured and normalized to values obtained from wells stimulated with 1 μM CpGA and peptide vehicle. Graphs represent data from $n = 3$ healthy donors measured in duplicate; error bars indicate SD. (**D**) Same as (B) except percentage of $BDCA2^+CD123^+$ pDCs with nuclear-localized IRF5 is shown after 4-hour stimulation with CpGA. One-way ANOVA with Bonferroni's multiple comparison test was performed.

and IRF5-CPP5 primarily interact with IRF5, and to a much lesser extent, IRF3, IRF7, and NF-κB (fig. S7D). Together, these data support that IRF5-CPPs are specifically binding to and inhibiting IRF5 activity.

IRF5-CPP2 inhibits CpGA-induced nuclear translocation of phosphorylated IRF5 in pDCs

Mechanistically, another possible explanation for the discord between IFNα inhibition and IRF5 nuclear translocation by IRF5-CPP2 could be at the level of IRF5 phosphorylation. Phosphorylation of IRF5 is a prerequisite for dimerization and nuclear translocation (*3*, *48*). Lopez-Pelaez *et al.* (*62*) and Ren *et al.* (*63*) recently identified inhibitor of NF-κB kinase β as a kinase that phosphorylates IRF5 at serine-462 (Ser^{462}) resulting in dimerization and nuclear translocation. Using a phospho-specific antibody that recognizes phosphorylated IRF5 at Ser^{462} (pIRF5), we examined whether CpGA could induce the nuclear translocation of pIRF5 in pDCs. Representative results in Fig. 6A show a time-dependent increase in nuclear-localized pIRF5 with translocation occurring as early as 30min after stimulation and

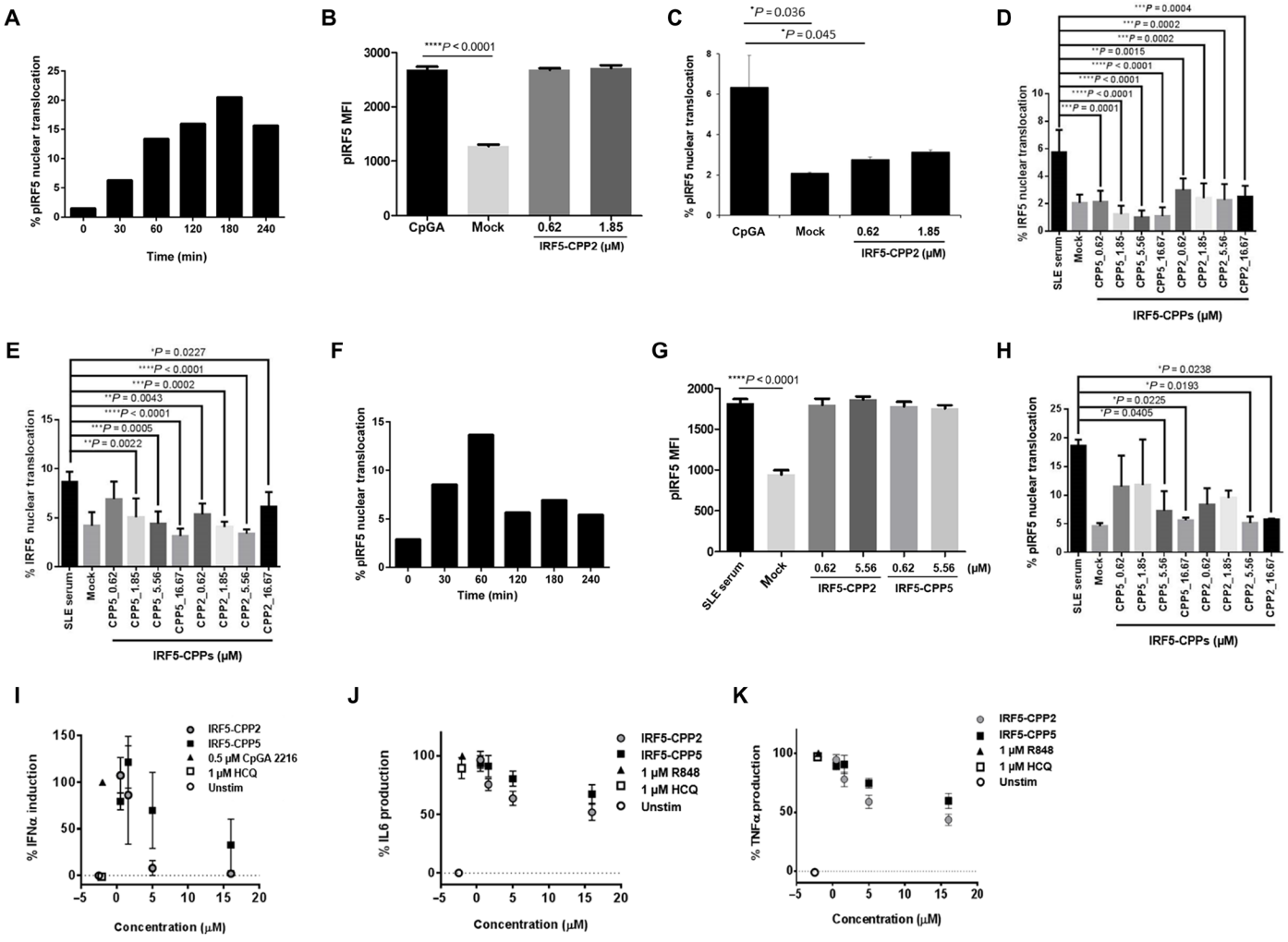

Fig. 6. IRF5-CPPs inhibit SLE serum–induced nuclear translocation of pIRF5 and TLR-mediated proinflammatory cytokine expression from SLE PBMCs. (**A**) Representative kinetic analysis of pIRF5 from imaging flow cytometry analysis. PBMCs were stimulated with CpGA over a time course and percentage of BDCA2$^+$CD123$^+$ pDCs with nuclear-localized pIRF5 plotted. Data are representative of three independent donors. (**B**) Similar to (A) except the effect of IRF5-CPP2 on CpGA-induced pIRF5 expression, measured as mean fluorescence intensity (MFI), is shown at 2 hours after stimulation. Data are from $n = 3$ independent healthy donors with SD. (**C**) Same as (B) except pIRF5 nuclear translocation is shown. (**D**) PBMCs were pretreated with IRF5-CPP2 or IRF5-CPP5 and stimulated with SLE serum for 2 hours. The percentage of CD14$^+$ monocytes (D) and CD19$^+$ B cells (**E**) with nuclear-localized IRF5 is shown. Data are from $n = 3$ independent healthy donors with SD. (**F**) Same as (A) except PBMCs were stimulated with SLE serum. Data are representative of three independent donors. (**G**) Similar to (B) except pIRF5 mean fluorescence intensity was measured in the presence or absence of IRF5-CPP2 and IRF5-CPP5 after 1-hour stimulation with SLE serum. Data are from $n = 3$ independent healthy donors with SD. (**H**) Same as (G) except nuclear-localized pIRF5 is shown. (**I** to **K**) SLE PBMCs were pretreated with IRF5-CPP2 or IRF5-CPP5 at various concentrations or 1 μM hydroxychloroquine (HCQ) and stimulated with 0.5 μM CpGA or 1 μM R848. IFNα (I), IL6 (J), and TNFα (K) levels in supernatant were measured and normalized to values obtained from wells stimulated with TLR ligand and peptide vehicle. Summarized data are from $n = 3$ SLE donors performed in triplicate; reported errors indicate SEM. One-way ANOVA with Bonferroni's multiple comparison test was performed.

peaking at 3 hours. The ability of IRF5-CPP2, over a low-concentration range, to inhibit CpGA-induced pIRF5 nuclear translocation was thus analyzed at 2 hours after stimulation. Somewhat unexpectedly, IRF5-CPP2 had no effect on the overall levels of pIRF5 induced by CpGA but, instead, resulted in the significant reduction of pIRF5 nuclear accumulation (Fig. 6, B and C).

IRF5-CPPs inhibit SLE serum–induced IRF5 activation and pIRF5 nuclear translocation

Given that IRF5 is constitutively activated in SLE monocytes and SLE serum stimulation of healthy monocytes replicated this finding (*37*), we examined the ability of IRF5-CPP2 and IRF5-CPP5 to inhibit SLE serum–induced IRF5 activation. PBMCs were stimulated with serum for 2 hours after 30-min preincubation with IRF5-CPP2 or IRF5-CPP5 and IRF5 cellular localization determined in CD14$^+$ monocytes. As expected, IRF5 nuclear translocation was increased by ~3-fold after SLE serum stimulation, and both IRF5-CPPs were active (Fig. 6D). Similar effects were seen in B cells where IRF5 nuclear translocation was increased ~2-fold with SLE serum and IRF5-CPPs inhibited IRF5 nuclear translocation in a dose-dependent manner (Fig. 6E).

To determine whether the kinetics of IRF5 activation (pIRF5) and inhibition differ between stimuli (a pure TLR ligand versus a more complex stimulus), PBMCs were stimulated over a time course with

SLE serum, and the kinetics of pIRF5 nuclear translocation were determined in pDCs. Quite notable, we found that the kinetics of IRF5 activation by SLE serum were much more rapid (Fig. 6F; peaking at 1 hour after stimulation) than by CpGA (Fig. 6A; peaking at 3 hours). These data suggest that distinct mechanisms of IRF5 activation may exist depending on the stimulation trigger. However, similar to data in Fig. 6 (B and C), concentration-dependent inhibition of pIRF5 nuclear translocation occurred in SLE serum–stimulated pDCs with no effect on overall levels of pIRF5 (Fig. 6, G and H). Downstream functional effects of IRF5-CPP2 and IRF5-CPP5 were then examined in SLE PBMCs after CpGA stimulation; both IRF5-CPPs exerted concentration-dependent inhibition of IFNα production (Fig. 6I and fig. S8A). Comparable findings were made after stimulation of SLE PBMCs with R848, resulting in the inhibition of IL6 and TNFα by CPP2 and CPP5 (Fig. 6, J and K, and fig. S8, B and C).

DISCUSSION

GWASs offer significant potential toward personalized medicine approaches for complex diseases (*22*). In addition to correlating genetic variation with risk of disease or biomarkers, it is important to directly assess biological function and determine therapeutic value of gene targeting. Novel approaches to identifying antagonists of these genes are necessary, especially if the candidate targets are transcription factors that are not suited for traditional targeting by small molecules or antibody-based drug discovery paradigms. One such approach is to identify CPP antagonists to facilitate drug discovery efforts (*64*). CPPs typically consist of 5 to 30 amino acids and have the ability to cross mammalian cell membranes and carry various cargo molecules with them. Although there is not a lot of clarity about specific features guiding cellular penetration, CPPs have been described to enter the cell through various mechanisms, including endocytosis and direct translocation (*65*). Here, we report the identification and evaluation of six novel IRF5-CPPs designed to disrupt protein-protein interactions considered critical for IRF5 homodimerization and function.

We leveraged a computational method generated at Roche (*49*) to design CPPs that target the transcription factor IRF5. On the basis of the dimeric structure of IRF5, we hypothesized that CPPs targeting Helix 2 or Helix 5 of IRF5 would disrupt dimerization and thereby offer novel tools to interrogate IRF5 function. We identified functional CPP motifs (Fig. 1B) and combined them with IRF5 sequences obtained from the dimeric crystal structure (*48*) to target IRF5 inhibition (Table 1). The computational approach has recently been published and serves as a valuable method to identify and design new CPPs (*49*). A postdesign workflow of testing CPPs in scalable biochemical and cell-based assays, as described here, will enable the determination of permeability, safety, selectivity, and biological function in human cells that would jumpstart drug discovery efforts around intriguing targets such as IRF5.

IRF5 is constitutively expressed in B cells, dendritic cells, monocytes, and macrophages and can be activated by virus infection, TLR signaling, DNA damage, and apoptotic/necrotic cell debris (*1*, *5*–*7*, *37*). Typically localized in the cytoplasm, IRF5 is activated upon phosphorylation and homodimerization, which results in nuclear translocation (*3*). Upon activation, IRF5 can cooperate with NF-κB to mediate the production of type I IFNs, as well as other proinflammatory cytokines (*61*). *Irf5*$^{-/-}$ mice display impaired production of proinflammatory cytokines, particularly TNFα, IL12, and IL6, and are thus resistant to endotoxic shock (*5*). Data presented here, using IRF5-CPPs in human cell-based assays, are in accordance with published reports supporting a role for IRF5 in TLR4-, TLR7/8-, and TLR9-induced proinflammatory cytokine production. GWASs have associated *IRF5* haplotypes with SLE risk (*23*–*26*) and high-serum IFNα levels (*35*). The main producers of type I IFNs are pDCs, and the role(s) of pDC-generated IFNα in SLE pathogenesis is well established (*66*). Thus, it is noteworthy that IRF5-CPPs were capable of inhibiting IFNα production (Figs. 5 and 6). These data are consistent with previous reports showing that IRF5 mediates TLR9 signaling in fms-like tyrosine kinase 3 (Flt-3)–induced murine pDCs (*67*). However, IRF5 likely promotes SLE pathogenesis through several pathways in addition to type I IFN production as *Irf5* deficiency prevented disease progression in the type I IFN receptor subunit 1–deficient FcγRIIB$^{-/-}$Yaa lupus model (*39*). IRF5 may contribute to the development of murine lupus, in part, by the secretion of pathogenic antibodies (*12*, *36*, *40*). In addition to inhibiting IRF5 function in human monocytes, pDCs, and B cells, we detected a notable disparity in IRF5-CPP2 and IRF5-CPP5 function in human MDMs. Only IRF5-CPP5 provided significant inhibition of human IRF5 in MDMs, and this was detected equally across all concentrations examined (3.5 to 15 μM). In contrast, IRF5-CPP2 was selective for the inhibition of murine Irf5 in BMDMs, but only at the highest dose of 15 μM, suggesting lower affinity for murine Irf5 (Fig. 4). On the basis of these data, it is tempting to speculate that the differential inhibition of human IRF5 by IRF5-CPP2 and IRF5-CPP5 in distinct cell types is due to their differential recognition of IRF5 isoforms. Human IRF5 is expressed as multiple alternatively spliced transcripts that encode for distinct IRF5 isoforms with cell type–specific expression (*38*, *68*); at least two murine Irf5 isoforms have been identified to date (*69*). Hence, the observed differences in potencies and functionalities of IRF5-CPPs between biochemical assays and cellular assays may be explained, in part, by the use of a single recombinant, purified IRF5, as compared to cellular IRF5 that exists in THP-1 cells and human primary PBMCs as multiple alternatively spliced isoforms (*68*). The further analysis of IRF5-CPP cell type–specific function(s) and direct binding to distinct IRF5 isoforms will be required to address this.

We assessed the specificity of IRF5-CPP2 and IRF5-CPP5 for human IRF5 by multiple independent assays. Depending on the assay, we used three different negative control peptides: CPP7 that contains only the YLK CPP sequence, IRF5-CPP8 that is the scrambled version of IRF5-CPP2, and IRF5-CPP9 that mimics IRF5-CPP5 but lacks the IRF5-specific residues. In all cases, these negative control peptides were unable to bind to IRF5, inhibit IRF5 dimerization, or inhibit IRF5 nuclear translocation. Although differences in potencies of IRF5-CPPs 1 to 6 were noted between biochemical and cellular assays, in most cases, data obtained between assays were well conserved. An exception to this was IRF5-CPP1 that showed low binding ability by biochemical assay (Fig. 1C and tables S1 and S2) yet provided significant cellular inhibition (Figs. 3A and 5, A and C). On the basis of these data, we would conclude that the observed functions for IRF5-CPP1 in cells are likely not IRF5 specific.

Conversely, results from homodimerization assays using either recombinant purified or endogenous protein, along with in-cell FRET and imaging flow cytometry, revealed that IRF5-CPP5 is a select inhibitor of human IRF5, more potent than IRF5-CPP2. Together with the analysis of IRF5-CPP function in murine BMDMs and the use of *Irf5*$^{-/-}$ BMDMs to further assess CPP specificity, we show that

IRF5-CPPs provide useful tools to interrogate immune cell functions regulated by human and murine IRF5, as well as provide greater insight into the mechanism(s) of IRF5 activation. In this regard, using pIRF5 antibodies directed against Ser^{462}, we found that the kinetics of endogenous IRF5 activation, via assessment of phosphorylation and nuclear translocation in human pDCs stimulated with CpGA or SLE serum, are distinct (Fig. 6, A and F). While these data suggest that different pathways of activation may be used downstream of these two IRF5-activating stimuli, they both resulted in the phosphorylation of Ser^{462}, in which mean fluorescence intensity of pIRF5 was similar between stimulated, untreated, and CPP-treated samples, and only pIRF5 nuclear translocation was inhibited by IRF5-CPP2 and IRF5-CPP5 (Fig. 6). Hence, inhibition of pIRF5 nuclear translocation rather than total IRF5 nuclear translocation by IRF5-CPP2 provided corroboration with the observed inhibition of IFNα production at 0.62 μM (Figs. 5C and 6C). Together, results from these studies support that IRF5-CPPs can be used for the in vitro analysis of IRF5 biologic function(s) that will allow for a thorough assessment of its therapeutic value as an autoimmune target. Ultimately, this type of strategy may be used to target other transcription factors, which are notoriously difficult to inhibit inside of the cell.

MATERIALS AND METHODS

Design of CPPs

A computational method to determine the likelihood that a peptide is a CPP (*49*) was built on the observation that CPPs can be separated from non-CPPs based on two key descriptors, hydrophobicity and polarity. Several hydrophobicity and/or polarity scales have been reported, with amino acids changing their relative ranking in each of these (*70*). We used the scale reported by Cruciani *et al.* (*71*), which is based on principal properties of amino acids. Unlike other hydrophobicity/polarity scales, we found that this scale could discriminate CPPs from non-CPPs. The dataset used included 109 CPPs and 1000 decoys. Decoys used were random peptides extracted from natural protein sequences that were expected to be noncell penetrating. As shown in Fig. 1B, decoys populate the CPP space (in green) only 1% of the time. IRF5 targeting CPPs 1 to 6 were designed on the basis of a modeled structure of the IRF5 dimer (Fig. 1A). We aimed to design CPPs that mimicked Helix 2 or Helix 5 to disrupt the formation of the dimer. Specifically, the following regions of IRF5 were selected:1)$IRF5_{455–464}$ (Connector)2)$IRF5_{455–478}$ (Connector + Helix 5)3)$IRF5_{465–478}$ (Helix 5)4)$IRF5_{323–336}$ (Helix 2)

Our computational analysis predicted that none of the native sequences were cell penetrating. The lack of cellular uptake was addressed by conjugating a peptide to a CPP. Additional novel strategies, including interweaving a CPP with a motif that is critical for binding and/or interweaving noncritical positions in IRF5-derived peptides with amino acids specifically selected to obtain an IRF5-targeting CPP, were used (fig. S1). On the basis of interactions between each IRF5 monomer in a model of the IRF5 dimer, we identified two critical binding motifs, I-L-IS-P--KD--V---K (Helix 5 + Connector) and Y---L--V (Helix 2). Specific sequences are shown in Table 1. IRF5-CPP1 was derived from $IRF5_{455–464}$ followed by the YLK CPP. IRF5-CPP2 is based on the I-L-IS-P--KD--V---K motif, with additional amino acids specifically selected to obtain a CPP. IRF5-CPPs 3 to 6 are based on the mPrP (1 to 28) CPP, interwoven with three key residues of Helix 2: Y---L—V. CPP7 contains only the YLK CPP sequence. IRF5-CPP8 is a scrambled version of IRF5-CPP2, and IRF5-CPP9 is identical to IRF5-CPP5 but lacks the IRF5-specific sequences.

Peptide synthesis

Peptides were synthesized by CSBio (Menlo Park, CA, USA) via solid phase using standard 9-fluorenylmethoxycarbonyl (Fmoc) protocols (*72*). All chemicals and solvents were purchased from VWR and Sigma-Aldrich and used as purchased without further purification. Mass spectra were recorded with electrospray ionization mode. The automated stepwise assembly of protected amino acids was constructed on a CS 336X series peptide synthesizer (CSBio, Menlo Park, CA, USA) with a Rink Amide MBHA resin C-terminal amide peptides or Wang resin for C-terminal carboxyl peptides as the polymer support. The protecting groups for Fmoc amino acids were as follows: Arg, (Pbf); Asn-Gln-Cys-His, (Trt); Asp-Glu, (OtBu); Lys-Trp, (Boc); Ser-Thr-Tyr, (t-Bu).

Fmoc-Rink amide resin or Fmoc-Wang resin (0.85 g, 0.4 mmol, sub: 0.47 mm/g) was mixed in a 25-ml reaction vessel (RV) with *N*,*N*′-dimethylformamide (DMF; 10 ml), and swollen for 10 to 30 min. The RV was mounted on a CS336 peptide automated synthesizer, and the amino acids were loaded onto the amino acid wheel according to the given peptide sequence. Hydroxybenzotriazole (HOBt) (0.5 M in DMF) and dissolved inorganic carbon (DIC; 0.5 M in DMF) were all predissolved separately in transferrable bottles under N_2. Fmoc–amino acids (4 equivalence, 1.6 mmol) were weighed and preloaded as powders on the amino acid wheel. Deprotection of the Fmoc group was carried out with 20% piperidine in DMF using the preset condition of the CS336 peptide synthesizer. Following seven washing cycles with 1:1 DMF/dichloromethane, amino acids were coupled using 1.6 mmol of HOBt and DIC in DMF. After shaking for 3 to 6 hours, the reaction mixture was filtered, and the resin was washed with DMF three times, followed by Fmoc deprotection according to the preset program using 20% pip in DMF. The coupling process was repeated with the respective building blocks until the last amino acid of a given sequence was coupled. Following the final amino acid coupling and deprotection, the peptide was cleaved from the resin or was acetylated with Ac_2O/*N*,*N*-diisopropylethylamine in DMF and then cleaved to give the desired product. Cleavage was achieved by treating final peptidyl resin (1 to 1.5 g) with a trifluoroacetic acid (TFA) cocktail (TFA/EDT/TIS/H_2O) at room temperature (RT) for 4 hours. The cleaved peptide was then filtered, and resin was washed with TFA. After precipitation with ethyl ether and washing, the crude peptide (200 to 500 mg) was obtained in a yield of 50 to 90% and a purity in the range of 30 to 70%. Further purification of the crude product was achieved by preparative high-performance liquid chromatography (HPLC) on a C18-column (250 mm by 46 mm, 10-μm particle size) with a linear gradient of 5 to 80% B (buffer A, 0.1% TFA /H2O; buffer B, acetonitrile) more than 60 min, with a flow rate of 25 to 40 ml/min. The appropriate fractions (purity, >90%) were lyophilized on a VirTis Freezemobile 35EL overnight to afford the pure product (fig. S9).

FITC-tagged analogs of IRF5-CPP2 and CPP5 were prepared (AnaSpec Inc., Fremont, CA, USA) using a similar solid-phase approach described above. The FITC label was conjugated to the N terminus of the peptides using a Long Chain (LC) linker, which is a six carbon linker/spacer of the 6-aminocaproic acid derivative. The final peptides (FITC-LC-MIILIISFPKHKDWKVILVK-OH and FITC-LC-MANLGYWLLALFVTYWTDLGLVKKRPKP-OH) were analyzed by HPLC and confirmed to be ≥95% pure. Molecular weights were

confirmed by liquid chromatography–mass spectrometry. Similar techniques were used to generate FITC-IRF5-CPP8 and FITC-IRF5-CPP9.

Thermal shift assay

One microliter of test peptide (0.62 mM IRF5-CPP1 or 0.31 mM IRF5-CPP2-CPP6) was added into polypropylene 384-well microplates (Thermal Scientific). A 25 μl of 2.48 μM His-IRF5 (222 to 425) in Assay Buffer [20 mM tris-HCl (pH 7.4), 100 mM NaCl, and 1 mM dithiothreitol (DTT)] was added. Plates were centrifuged for 1 min at 1200 rpm (Eppendorf Centrifuge 5810 R) and incubated on a plate shaker at RT for 10 min. Five microliters of 25× Sypro Orange Dye (Invitrogen) diluted from the 5000× stock in Assay Buffer was added. After the plates were incubated at RT for 2 min, 20 μl per well of above reaction was transferred into Hard-Shell 384-well polymerase chain reaction (PCR) plates (Bio-Rad), followed by overlaying with 10 μl of mineral oil (Sigma-Aldrich) to prevent evaporation. The assay signals were monitored by reading excitation at 465 nm and emission fluorescence at 590 nm on a FluoDiaT70 reader (Photon Technology International) every 1.5°C increments from 30° to 55.5°C with a total of 18 reads. The fluorescence intensity signals fitted to Boltzmann equation were plotted using GraphPad Prism software.

K_D determination of FITC-CPP binding to IRF5

Aliquots (1.6 μl per well) of 4 μM FITC peptide solution in dimethyl sulfoxide (DMSO) were added to 96-well polypropylene plates (Corning). Thirty microliter per well of various concentrations (0 to 10.5 μM, twofold serial dilution) of recombinant His-tag IRF5 (222 to 425) in Assay Buffer [50 mM tris-HCl (pH 7.4), 100 mM NaCl, 1 mM DTT, and bovine serum albumin (BSA; 0.2 mg/ml)] were added to FITC peptide–containing wells and incubated at RT for 30 min. Ten microliters per well of different concentrations of Terbium (Tb)–labeled anti-His antibody in Assay Buffer (without DTT) were added into wells containing corresponding concentrations of IRF5 solution to keep the same ratio of IRF5 to Tb (10:1). Samples were incubated at 4°C for overnight, and 18 μl per well were transferred to 384-well polystyrene plates (Corning) in duplicates. Assay signals were monitored by reading excitation at 340 nm and emission fluorescence at 495 and 525 nm on an EnVision reader. The TR-FRET signals were calculated from the fluorescence intensities at 525 nm after subtracting the background from assay buffer. The data were processed in Prism software (GraphPad), and K_D values were calculated using one site-specific binding algorithm.

Recombinant IRF5 dimerization assay

Recombinant IRF5 dimerization was measured by TR-FRET. Test peptides (2 mM stock in DMSO) were diluted threefold in DMSO and 2.5 μl per well added into 96-well polypropylene plates. Fifty microliters per well of 100 nM recombinant biotin-tag IRF5(222 to 467, S430D) and 250 nM recombinant His-tag IRF5(222 to 467, S430D) in Assay Buffer [50 mM tris-HCl (pH 7.4), 100 mM NaCl, 1 mM DTT, and BSA (0.2 mg/ml)] were added. Samples were incubated at RT for 20 min. Detection solution (17 μl per well) containing 10 nM europium-conjugated streptavidin and 80 nM allophycocyanin-conjugated anti–glutathione *S*-transferase antibody (Columbia Biosciences) in Assay Buffer (without DTT) were added. Samples were incubated at RT for 60 min followed by overnight incubation at 4°C, and 30 μl per well were transferred to 384-well polystyrene plates. Assay signals were monitored by reading excitation at 340 nm and emission fluorescence at 615 and 665 nm on an EnVision reader. Data were processed in Excel XLfit, and IC_{50} values were calculated using a nonlinear curve-fitting algorithm (four parameter equation; table S2).

Cells and stimulations

HeLa (CCL-2) and THP-1 cells (TIB-202) were purchased from American Type Culture Collection and cultured using standard methods. PBMCs were isolated from whole blood of healthy donors or patients with SLE as described (*37*). All human blood samples were obtained with informed consent and strict adherence to institutional review board policies. A total of 100,000 PBMCs per well of 96-well plates were plated in RPMI 1640 media with 10% fetal bovine serum (FBS), pretreated with IRF5-CPPs for 30 min, then stimulated with 1 μM R848 (Enzo, ALX-420-038-M005), and incubated at 37°C overnight. pDCs were isolated from leukopaks obtained from New York Blood Center using the Miltenyi Diamond pDC kit. pDC purity, as determined by flow cytometry, was >70%. Five thousand pDCs per well were plated, pretreated with IRF5-CPPs, and stimulated with 1 μM CpGA (InvivoGen, ODN 2336) overnight. Total B cells were isolated using the B cell Isolation Kit (Miltenyi). B cells with a purity of >90% were used in experiments. A total of 100,000 cells per well were plated in RPMI 1640 with 10% FBS and 100 μl of IL2 and then pretreated with peptides and 100 nM CpGB (Hycult, HC4039). Human MDMs were in vitro derived as follows: Monocytes were isolated using the Pan Monocyte Isolation Kit (Miltenyi, 130-096-537); purity was determined to be >95% by flow cytometry. In a 96-well flat bottom plate, 2×10^5 monocytes per well were plated in Iscove's modified Dulbecco's media with 10% human AB serum and recombinant human granulocyte-macrophage colony-stimulating factor (100 ng/ml; R&D, 215-GM) and then cultured for 7 days to generate MDMs. On day 7, cells were starved for 2 hours, preincubated with peptides for 1 hour, and then treated with LPS (1 ng/ml; Sigma-Aldrich, L5293) or 3 μM R848 (InvivoGen, tlrl-r848). Cells and supernatants were collected at 4 and 24 hours after stimulation. In a similar manner, murine BMDMs were generated from red blood cell–lysed bone marrow cells from femur and tibia of age (8 to 12 weeks old) and gender-matched *Irf5*$^{-/-}$ and littermate-matched WT (*Irf5*$^{+/+}$) Balb/c mice (*73*). Following 6 days of differentiation with macrophage colony-stimulating factor and L929-conditioned media, 1×10^6 cells were plated, preincubated with peptides, and then treated with LPS (40 μg/ml) or R848 (100 ng/ml). Cells and supernatants were collected at 4 and 24 hours after stimulation. SLE PBMCs were from Sanguine Biosciences (Sherman Oaks, CA). A total of 100,000 cells per well were plated in 96-well U-bottom plates in RPMI 1640, supplemented with 10% FBS, 2 mM L-glutamine, penicillin-streptomycin (100 IU/ml), 1 mM sodium pyruvate, 55 μM β-mercaptoethanol, 0.01 M Hepes, and 1% nonessential amino acids. Cells were pretreated for 30 min with IRF5-CPPs or 1 μM chloroquine (InvivoGen, tlrl-chq). Cells were then stimulated with 1 μM R848 (Enzo, ALX-420-038-M005) or 0.5 μM CpGA 2216 (InvivoGen, ODN 2216) and incubated at 37°C with 5% CO_2 for 18 to 20 hours. Peptides were dissolved in DMSO as 10 mM stock solutions and then diluted 1:10 in water to achieve 1 mM solution. CPP dilutions were added to 96-well cell plates and incubated 30 min at 37°C before addition of stimulus.

Intracellular IRF5 dimerization assay

For intracellular FRET, THP-1 cells were incubated with 1 μM FITC-conjugated IRF5-CPPs for 1 hour, fixed, permeabilized, and

stained with anti-IRF3 (Abcam, ab76409), anti-IRF5 (ab124792; or Cell Signaling Technology, cs13496), anti-IRF7 (cs4920), or anti–NF-κB (cs8242) antibodies and TRITC-conjugated secondary antibodies (Abcam). Cell-associated fluorescence was measured on BioTek Synergy Neo2 (BioTek, VT) at 525 nm upon excitation at 488 nm (E1), at 600 nm after excitation at 540 nm (E2), and at 600 nm after excitation at 488 nm (E3). The transfer of fluorescence was calculated as FRET units as follows: FRET unit = ($E3_{both} - E3_{none}$) − ([$E3_{TRITC} - E3_{none}$) × ($E2_{both}/E2_{TRITC}$]) − ([$E3_{FITC} - E3_{none}$] × [$E1_{both}/E1_{FITC}$]) (*53*). The different fluorescence values (E) were measured on unlabeled cells (E_{none}) or cells labeled with FITC (E_{FITC}) and TRITC (E_{TRITC}). In a similar manner, FRET signal was analyzed by imaging flow cytometry on an ImageStreamX Mark II (EMD Millipore), and FITC-TRITC similarity scores were determined using IDEAS software package (*55*).

IRF3, IRF5, and IRF7 homodimerization were determined by Native gel electrophoresis after preincubation of THP-1 monocytes with IRF5-CPPs (1 and 10 μM) and stimulation with R848 for 1 hour. An 8% Native gel was prerun in 25 mM tris/192 mM glycine (pH 8.3) with 1% (w/v) deoxycholate in the cathode chamber for 30 min at 40 mA at 0°C. Cell lysates (10 μg) were mixed with Native sample buffer [62.5 mM tris-Cl (pH 6.8), 15% glycerol, and 1% bromophenol blue) and electrophoresed for 60 min at 25 mA and 0°C. The gel was then incubated for 30 min with 25 mM tris/192 mM glycine (pH 8.3) and 0.1% SDS before protein transfer. Homodimer and monomer IRFs and β-actin were detected with anti-IRF3 (ab76409), anti-IRF5 (cs3257 or cs13496), or anti-IRF7 (cs4920) and horseradish peroxidase (HRP)–conjugated monoclonal anti–β-actin (cs5125) antibodies, respectively.

Nuclear translocation assays

The ability of CPPs to inhibit NF-κB nuclear translocation was determined by confocal microscopy and imaging flow cytometry. For confocal, HeLa cells were plated at 5000 cells per well in 96-well ViewPlates and incubated overnight at 37°C. Medium was aspirated and prediluted compounds in 0.05% BSA Hanks/20 mM Hepes added and incubated for 30 min. Wells were stimulated with 20 μl of TNFα (150 ng/ml) for 30 min at 37°C and aspirated, and cells were fixed with 3.7% formaldehyde solution for 15 min. NF-κB translocation, based on detection of the p65 subunit, was determined on the PerkinElmer Operetta at 20×. IRF5, IRF7, and NF-κB nuclear translocation were analyzed by imaging flow cytometry. Representative gating strategy is shown in fig. S4A. For NF-κB and IRF7, 4×10^6 PBMCs were stimulated with R848 or CpGA, surface-stained with anti-CD14 or anti-CD123 and anti-BDCA2 antibodies to detect monocytes and pDCs, respectively, fixed, and permeabilized for intracellular staining with preconjugated anti–NF-κB and anti-IRF7 antibodies (Santa Cruz Biotechnology). For total IRF5 and p(Ser^{462})IRF5, 8×10^6 PBMCs were stimulated with either R848 for 2 hours and surface-stained with anti-CD19 and anti-CD14 to detect B cells and monocytes, respectively, or stimulated with CpGA for 4 hours and surface-stained with pDC markers. After fixation of B cells and monocytes, intracellular IRF5 was detected with preconjugated anti-IRF5 (FITC) antibodies (ab193245) for total IRF5 or anti-p(Ser^{462})IRF5 (provided by MRC Protein Phosphorylation and Ubiquitylation Unit Reagents; https://mrcppureagents.dundee.ac.uk) with Alexa Fluor (AF) 488 secondary antibodies for pIRF5. For pDCs, IRF5 was detected with preconjugated anti-IRF5 (AF647) antibodies (ab192983) and anti-p(Ser^{462})IRF5 antibodies. Before acquisition, the nuclear dye DRAQ5 (BioStatus) was added. Images were acquired on the ImageStream using the 40× objective; nuclear translocation was quantified using the Similarity Score feature within the IDEAS software package (*37*).

The effect of IRF5-CPPs on IRF5 nuclear translocation was confirmed by Western blot analysis of nuclear extracts from human primary monocytes stimulated with R848. Monocytes were purified using the EasySep Isolation Kit (STEMCELL Technologies, 19359) and then preincubated with 1 and 10 μM CPP2 or CPP5 for 30 min before stimulating with phosphate-buffered saline (PBS) or R848 (500 ng/ml) for 2 hours. Cells were fractionated according to the manufacturer's instruction (Cell Fractionation Kit, cs9038). Following fractionation, lysates were sonicated and boiled. Nuclear fraction was analyzed by Western blot as follows: 30 μl of lysate was loaded onto a 3 to 8% NuPAGE Novex Tris-Acetate gel (Life Technologies, EA0378BOX) and transferred onto a 0.45-μm nitrocellulose membrane (Bio-Rad Laboratories). Membrane was blocked in tris-buffered saline/0.25% Tween 20 containing 5% BSA for 1 hour at RT and incubated overnight at 4°C with anti-IRF5 antibodies (cs13496), followed by HRP-conjugated secondary antibody (cs7074). The nuclear fraction was confirmed using Lamin B1 (cs15068). Membrane was incubated with Clarity ECL Western Blotting Substrate (Bio-Rad Laboratories) and chemiluminescence detected with a ChemiDoc MP Imaging System (Bio-Rad Laboratories). The PageRuler Plus Prestained Protein Ladder (Thermo Fisher Scientific) was used for size reference.

Cell internalization and colocalization assays

The ability of FITC-tagged CPPs to penetrate cells was determined by confocal microscopy and imaging flow cytometry. For confocal, 5000 HeLa cells per well were plated onto Whatman glass-bottom 96-well plates for FITC uptake. Twenty-four hours after plating, peptides were added. At 2 and 24 hours after addition, medium was removed, and cells were washed with acidic saline (50 μl per well; pH 3) and fixed with 37°C fixative (19.9 ml of Hanks/Hepes per 2.2 ml of formaldehyde) for 15 min, followed by PBS. Cellular uptake of FITC-labeled peptides was assessed by automated confocal microscopy and images obtained at ×40 magnification. For imaging flow, 8×10^6 primary purified PBMCs were incubated with FITC-tagged CPPs for 1 hour, and cells were surface-stained with anti-CD14, anti-CD19, and anti-CD123/anti-BDCA2 antibodies to measure FITC uptake and localization in each cell population (*37*). Colocalization of FITC-tagged CPPs with endogenous IRF5 was analyzed after permeabilization and intracellular staining with anti-IRF5 (AF647) antibodies. Analysis was performed using the Bright Detail Similarity feature and the Internalization feature within IDEAS software package.

Enzyme-linked immunosorbent assay

Culture supernatants from SLE PBMCs and MDMs were collected and analyzed for IL6, IL1b, TNFα, IFNα, IFN-γ, IL10, IL12p70, and IgG levels by AlphaLISA (PerkinElmer, AL223C, AL220C, AL208C, AL217C, AL217C, AL218C, AL3116C, and AL205C, respectively). IL12p40 levels were measured using the Quantikine ELISA Kit (R&D Systems, DP400). In a similar manner, MDM culture supernatants were collected and analyzed for IL6 levels by AlphaLISA (PerkinElmer, AL567C), and IL10, TNFα and TGFβ levels were measured by Quantikine ELISA kits (R&D Systems; M100B, MTA00B, and MB100B, respectively). Levels were normalized to values obtained from wells stimulated with 1 μM R848, 1 μM CpGB (InvivoGen,

ODN 2006), or 100 nM CpGA and peptide vehicle (0.05% DMSO and 5% water).

RNA extraction, complementary DNA synthesis, and quantitative real-time PCR

Cells from the in vitro human macrophage assays (described above) were lysed with RLT buffer (Qiagen) with β-mercaptoethanol. Total RNA was extracted using the RNA isolation kit (RNeasy 96) as per the manufacturer's instructions (QIAGEN). Thereafter, complementary DNA (cDNA) was synthesized using the High-Capacity cDNA Reverse Transcription Kit supplemented with ribonuclease inhibitor (Invitrogen). For quantitative real-time PCR, all reactions were performed with the Universal PCR master mix and predesigned TaqMan primers and probes (Invitrogen). Thermal cycling was run under the TaqMan Fast program on a QuantStudio instrument (Applied Biosystems). Primer pairs used in this study are listed in table S3. Gene expression analysis was conducted using a comparative threshold cycle method ($\Delta\Delta C_t$) with normalization to housekeeping genes glyceraldehyde-3-phosphate dehydrogenase and beta actin.

Statistical analyses

Experimental replicates ($\geq$3) were used unless otherwise noted. For comparisons of one factor over multiple groups, one-way analysis of variance (ANOVA) was performed with Bonferroni's post hoc test. Statistical analysis was performed using GraphPad Prism (version 7.0). Data are reported as means ± SD or medians ± SEM.

SUPPLEMENTARY MATERIALS

Supplementary material for this article is available at http://advances.sciencemag.org/cgi/content/full/6/20/eaay1057/DC1

View/request a protocol for this paper from *Bio-protocol*.

REFERENCES AND NOTES

1. B. J. Barnes, P. A. Moore, P. M. Pitha, Virus-specific activation of a novel interferon regulatory factor, IRF-5, results in the induction of distinct interferon α genes. *J. Biol. Chem.* **276**, 23382–23390 (2001).
2. B. J. Barnes, M. J. Richards, M. Mancl, S. Hanash, L. Beretta, P. M. Pitha, Global and distinct targets of IRF-5 and IRF-7 during innate response to viral infection. *J. Biol. Chem.* **279**, 45194–45207 (2004).
3. B. J. Barnes, M. J. Kellum, A. E. Field, P. M. Pitha, Multiple regulatory domains of IRF-5 control activation, cellular localization and induction of chemokines that mediate T-lymphocyte recruitment. *Mol. Cell. Biol.* **22**, 5721–5740 (2002).
4. B. J. Barnes, M. J. Kellum, K. E. Pinder, J. A. Frisancho, P. M. Pitha, IRF-5, a novel mediator of cell-cycle arrest and cell death. *Cancer Res.* **63**, 6424–6431 (2003).
5. A. Takaoka, H. Yanai, S. Kondo, G. Duncan, H. Negishi, T. Mizutani, S. Kano, K. Honda, Y. Ohba, T. W. Mak, T. Taniguchi, Integral role of IRF-5 in the gene induction programme activated by Toll-like receptors. *Nature* **434**, 243–249 (2005).
6. A. Schoenemeyer, B. J. Barnes, M. E. Mancl, E. Latz, N. Goutagny, P. M. Pitha, K. A. Fitzgerald, D. T. Golenbock, The interferon regulatory factor, IRF5, is a central mediator of toll-like receptor 7 signaling. *J. Biol. Chem.* **280**, 17005–17012 (2005).
7. G. Hu, M. E. Mancl, B. J. Barnes, Signaling through IFN regulatory factor-5 sensitizes p53-deficient tumors to DNA damage-induced apoptosis and cell death. *Cancer Res.* **65**, 7403–7412 (2005).
8. G. Hu, B. J. Barnes, IRF-5 is a mediator of the death receptor-induced apoptotic signaling pathway. *J. Biol. Chem.* **284**, 2767–2777 (2009).
9. H. Yanai, H. M. Chen, T. Inuzuka, S. Kondo, T. W. Mak, A. Takaoka, K. Honda, T. Taniguchi, Role of IFN regulatory factor 5 transcription factor in antiviral immunity and tumor suppression. *Proc. Natl. Acad. Sci. U.S.A.* **104**, 3402–3407 (2007).
10. A. Couzinet, K. Tamura, H. M. Chen, K. Nishimura, Z. Wang, Y. Morishita, K. Takeda, H. Yagita, H. Yanai, T. Taniguchi, T. Tamura, A cell-type-specific requirement for IFN regulatory factor 5 (IRF5) in Fas-induced apoptosis. *Proc. Natl. Acad. Sci. U.S.A.* **105**, 2556–2561 (2008).
11. T. Krausgruber, K. Blazek, T. Smallie, S. Alzabin, H. Lockstone, N. Sahgal, T. Hussell, M. Feldmann, I. A. Udalova, IRF5 promotes inflammatory macrophage polarization and T_H1-T_H17 responses. *Nat. Immunol.* **12**, 231–238 (2011).
12. S. De, B. Zhang, T. Shih, S. Singh, A. Winkler, R. Donnelly, B. J. Barnes, B cell-intrinsic role for IRF5 in TLR9/BCR-induced human B cell activation, proliferation, and plasmablast differentiation. *Front. Immunol.* **8**, 1938 (2018).
13. X. Bi, M. Hameed, N. Mirani, E. M. Pimenta, J. Anari, B. J. Barnes, Loss of interferon regulatory factor 5 (IRF5) expression in human ductal carcinoma correlates with disease stage and contributes to metastasis. *Breast Cancer Res.* **13**, R111 (2011).
14. V. Fresquet, E. F. Robles, A. Parker, J. Martinez-Useros, M. Mena, R. Malumbres, X. Agirre, S. Catarino, D. Arteta, L. Osaba, M. Mollejo, J. M. Hernandez-Rivas, M. J. Calasanz, M. Daibata, M. J. Dyer, F. Prosper, E. Vizcarra, M. A. Piris, D. Oscier, J. A. Martinez-Climent, High-throughput sequencing analysis of the chromosome 7q32 deletion reveals IRF5 as a potential tumour suppressor in splenic marginal-zone lymphoma. *Br. J. Haematol.* **158**, 712–726 (2012).
15. T. Masuda, S. Iwamoto, R. Yoshinaga, H. Tozaki-Saitoh, A. Nishiyama, T. W. Mak, T. Tamura, M. Tsuda, K. Inoue, Transcription factor IRF5 drives $P2X4R^+$-reactive microglia gating neuropathic pain. *Nat. Commun.* **5**, 3771 (2014).
16. G. Courties, T. Heidt, M. Sebas, Y. Iwamoto, D. Jeon, J. Truelove, B. Tricot, G. Wojtkiewicz, P. Dutta, H. B. Sager, A. Borodovsky, T. Novobrantseva, B. Klebanov, K. Fitzgerald, D. G. Anderson, P. Libby, F. K. Swirski, R. Weissleder, M. Nahrendorf, In vivo silencing of the transcription factor IRF5 reprograms the macrophage phenotype and improves infarct healing. *J. Am. Coll. Cardiol.* **63**, 1556–1566 (2014).
17. S. Kreher, M. A. Bouhlel, P. Cauchy, B. Lamprecht, S. Li, M. Grau, F. Hummel, K. Kochert, I. Anagnostopoulos, K. Johrens, M. Hummel, J. Hiscott, S. S. Wenzel, P. Lenz, M. Schneider, R. Kuppers, C. Scheidereit, M. Giefing, R. Siebert, K. Rajewsky, G. Lenz, P. N. Cockerill, M. Janz, B. Dörkern, C. Bonifer, S. Mathas, Mapping of transcription factor motifs in active chromatin identifies IRF5 as key regulator in classical Hodgkin lymphoma. *Proc. Natl. Acad. Sci. U.S.A.* **111**, E4513–E4522 (2014).
18. M. Weiss, A. J. Byrne, K. Blazek, D. G. Saliba, J. E. Pease, D. Perocheau, M. Feldmann, I. A. Udalova, IRF5 controls both acute and chronic inflammation. *Proc. Natl. Acad. Sci. U.S.A.* **112**, 11001–11006 (2015).
19. A. A. Watkins, K. Yasuda, G. E. Wilson, T. Aprahamian, Y. Xie, E. Maganto-Garcia, P. Shukla, L. Oberlander, B. Laskow, H. Menn-Josephy, Y. Wu, P. Duffau, S. K. Fried, A. H. Lichtman, R. G. Bonegio, I. R. Rifkin, IRF5 deficiency ameliorates lupus but promotes atherosclerosis and metabolic dysfunction in a mouse model of lupus-associated atherosclerosis. *J. Immunol.* **194**, 1467–1479 (2015).
20. E. Dalmas, A. Toubal, F. Alzaid, K. Blazek, H. L. Eames, K. Lebozec, M. Pini, I. Hainault, E. Montastier, R. G. P. Denis, P. Ancel, A. Lacombe, Y. Ling, O. Allatif, C. Cruciani-Guglielmacci, S. Andre, N. Viguerie, C. Poitou, V. Stich, A. Torcivia, F. Foufelle, S. Luquet, J. Aron-Wisnewsky, D. Langin, K. Clement, I. A. Udalova, N. Venteclef, Irf5 deficiency in macrophages promotes beneficial adipose tissue expansion and insulin sensitivity during obesity. *Nat. Med.* **21**, 610–618 (2015).
21. A. Fabié, L. T. Mai, X. Dagenais-Lussier, A. Hammami, J. van Grevenynghe, S. Stäger, IRF-5 promotes cell death in CD4 T cells during chronic infection. *Cell Rep.* **24**, 1163–1175 (2018).
22. L. Tang, B. Chen, B. Ma, S. Nie, Association between IRF5 polymorphisms and autoimmune diseases: A meta-analysis. *Genet. Mol. Res.* **13**, 4473–4485 (2014).
23. S. Sigurddson, G. Nordmark, H. H. Göring, K. Lindroos, A. C. Wiman, G. Sturfelt, A. Jonsen, S. Rantapaa-Dahlqvist, B. Moller, J. Kere, S. Koskenmies, E. Widen, M. L. Eloranta, H. Julkunen, H. Kristjansdottir, K. Steinsson, G. Alm, L. Ronnblom, A. C. Syvänen, Polymorphisms in the tyrosine kinase 2 and interferon regulatory factor 5 genes are associated with systemic lupus erythematosus. *Am. J. Hum. Genet.* **76**, 528–537 (2005).
24. S. Sigurdsson, H. H. Göring, G. Kristjansdottir, L. Milani, G. Nordmark, J. K. Sandling, M. L. Eloranta, D. Feng, N. Sangster-Guity, I. Gunnarsson, E. Svenungsson, G. Sturfelt, A. Jonsen, L. Truedsson, B. J. Barnes, G. Alm, L. Ronnblom, A. C. Syvänen, Comprehensive evaluation of the genetic variants of interferon regulatory factor 5 reveals a novel 5bp length polymorphism as strong risk factor for systemic lupus erythematosus. *Hum. Mol. Genet.* **17**, 872–881 (2008).
25. R. R. Graham, S. V. Kozyrev, E. C. Baechler, M. V. P. L. Reddy, R. M. Plenge, J. W. Bauer, W. A. Ortmann, T. Koeuth, M. F. González Escribano; Argentine and Spanish Collaborative Groups, B. Pons-Estel, M. Petri, M. Daly, P. K. Gregersen, J. Martín, D. Altshuler, T. W. Behrens, M. E. Alarcón-Riquelme, A common haplotype of interferon regulatory factor 5 (IRF5) regulates splicing and expression and is associated with increased risk of systemic lupus erythematosus. *Nat. Genet.* **38**, 550–555 (2006).
26. R. R. Graham, C. Kyogoku, S. Sigurdsson, I. A. Vlasova, L. R. Davies, E. C. Baechler, R. M. Plenge, T. Koeuth, W. A. Ortmann, G. Hom, J. W. Bauer, C. Gillett, N. Burtt, D. S. Cunninghame Graham, R. Onofrio, M. Petri, I. Gunnarsson, E. Svenungsson, L. Ronnblom, G. Nordmark, P. K. Gregersen, K. Moser, P. M. Gaffney, L. A. Criswell, T. J. Vyse, A. C. Syvänen, P. R. Bohjanen, M. J. Daly, T. W. Behrens, D. Altshuler, Three functional variants of IFN regulatory factor 5 (IRF5) define risk and protective haplotypes for human lupus. *Proc. Natl. Acad. Sci. U.S.A.* **104**, 6758–6763 (2007).
27. C. Miceli-Richard, N. Gestermann, M. Ittah, E. Comets, P. Loiseau, X. Puechal, E. Hachulla, J. E. Gottenberg, P. Lebon, L. Becquemont, X. Mariette, The CGGGG insertion/deletion polymorphism of the IRF5 promoter is a strong risk factor for primary Sjögren's syndrome. *Arthritis Rheum.* **60**, 1991–1997 (2009).

28. G. M. Hirschfield, X. Liu, Y. Han, I. P. Gorlov, Y. Lu, C. Xu, Y. Lu, W. Chen, B. D. Juran, C. Coltescu, A. L. Mason, P. Milkiewicz, R. P. Myers, J. A. Odin, V. A. Luketic, D. Speiciene, C. Vincent, C. Levy, P. K. Gregersen, J. Zhang, E. J. Heathcote, K. N. Lazaridis, C. I. Amos, K. A. Siminovitch, Variants at IRF5-TNPO3, 17q12-21 and MMEL1 are associated with primary biliary cirrhosis. *Nat. Genet.* **42**, 655–657 (2010).
29. B. Rueda, M. V. Reddy, M. A. Gonzalez-Gay, A. Balsa, D. Pascual-Salcedo, I. F. Petersson, A. Eimon, S. Paira, H. R. Scherbartch, B. A. Pons-Estel, M. F. Gonzalez-Escribano, M. E. Alarcon-Riquelme, J. Martín, Analysis of IRF5 gene functional polymorphisms in rheumatoid arthritis. *Arthritis Rheum.* **54**, 3815–3819 (2006).
30. V. Dideberg, G. Kristjansdottir, L. Milani, C. Libioulle, S. Sigurdsson, E. Louis, A. C. Wiman, S. Vermeire, P. Rutgeerts, J. Belaiche, D. Franchimont, A. Van Gossum, V. Bours, A. C. Syvänen, An insertion-deletion polymorphism in the interferon regulatory factor 5 (IRF5) gene confers risk of inflammatory bowel disease. *Hum. Mol. Genet.* **16**, 3008–3016 (2007).
31. M. Garcia-Bermudez, R. Lopez-Mejias, F. Genre, S. Castaneda, J. Llorca, C. Gonzalez-Juanatey, A. Corrales, B. Ubilla, J. A. Miranda-Filloy, T. Pina, C. Gomez-Vaquero, L. Rodriguez-Rodriguez, B. Fernandez-Gutierrez, A. Balsa, D. Pascual-Salcedo, F. J. Lopez-Longo, P. Carreira, R. Blanco, J. Martin, M. A. Gonzalez-Gay, Interferon regulatory factor 5 genetic variants are associated with cardiovascular disease in patients with rheumatoid arthritis. *Arthritis Res. Ther.* **16**, R146 (2014).
32. R. Saigusa, Y. Asano, T. Taniguchi, T. Yamashita, Y. Ichimura, T. Takahashi, T. Toyama, A. Yoshizaki, K. Sugawara, D. Tsuruta, T. Taniguchi, S. Sato, Multifaceted contribution of the TLR4-activated IRF5 transcription factor in systemic sclerosis. *Proc. Natl. Acad. Sci. U.S.A.* **112**, 15136–15141 (2015).
33. C. Rahmattulla, A. L. Mooyaart, D. van Hooven, J. W. Schoones, J. A. Bruijn, O. M. Dekkers; European Vasculitis Genetics Consortium, I. M. Bajema, Genetic variants in ANCA-associated vasculitis: A meta-analysis. *Ann. Rheum. Dis.* **75**, 1687–1692 (2016).
34. D. Feng, R. C. Stone, M. L. Eloranta, N. Sangster-Guity, G. Normark, S. Sigurdsson, C. Wang, A. C. Syvänen, L. Rönnblom, B. J. Barnes, Genetic variants and disease-associated factors contribute to enhanced interferon regulatory factor 5 expression in blood cells of patients with systemic lupus erythematosus. *Arthritis Rheum.* **62**, 562–573 (2010).
35. T. B. Niewold, J. A. Kelly, M. H. Flesch, L. R. Espinoza, J. B. Harley, M. K. Crow, Association of the IRF5 risk haplotype with high serum interferon-α activity in systemic lupus erythematosus patients. *Arthritis Rheum.* **58**, 2481–2487 (2008).
36. D. Feng, L. Yang, X. Bi, R. C. Stone, P. Patel, B. J. Barnes, *Irf5*-deficient mice are protected from pristane-induced lupus via increased Th2 cytokines and altered IgG class switching. *Eur. J. Immunol.* **42**, 1477–1487 (2012).
37. R. C. Stone, D. Feng, J. Deng, S. Singh, L. Yang, P. Fitzgerald-Bocarsly, M. L. Eloranta, L. Ronnblom, B. J. Barnes, Interferon regulatory factor 5 activation in monocytes of systemic lupus erythematosus patients is triggered by circulating autoantigens independent of type I interferons. *Arthritis Rheum.* **64**, 788–798 (2012).
38. R. C. Stone, P. Du, D. Feng, K. Dhawan, L. Ronnblom, M. L. Eloranta, R. Donnelly, B. J. Barnes, RNA-seq for enrichment and analysis of IRF5 transcript expression in SLE. *PLOS ONE* **8**, e54487 (2013).
39. C. Richez, K. Yasuda, R. G. Bonegio, A. A. Watkins, T. Aprahamian, P. Busto, R. J. Richards, C. L. Liu, R. Cheung, P. J. Utz, A. Marshak-Rothstein, I. R. Rifkin, IFN regulatory factor 5 is required for disease development in the *FcγRIIB*$^{-/-}$*Yaa* and *FcγRIIB*$^{-/-}$ mouse models of systemic lupus erythematosus. *J. Immunol.* **184**, 796–806 (2010).
40. D. A. Savitsky, H. Yanai, T. Tamura, T. Taniguchi, K. Honda, Contribution of IRF5 in B cells to the development of murine SLE-like disease through its transcriptional control of the IgG2a locus. *Proc. Natl. Acad. Sci. U.S.A.* **107**, 10154–10159 (2010).
41. Y. Tada, S. Kondo, S. Aoki, S. Koarada, H. Inoue, R. Suematsu, A. Ohta, T. W. Mak, K. Nagasawa, Interferon regulatory factor 5 is critical for the development of lupus in MRL/lpr mice. *Arthritis Rheum.* **63**, 738–748 (2011).
42. L. Yang, D. Feng, X. Bi, R. C. Stone, B. J. Barnes, Monocytes from *Irf5*$^{-/-}$ mice have an intrinsic defect in their response to pristane-induced lupus. *J. Immunol.* **189**, 3741–3750 (2012).
43. B. J. Barnes, Genetic versus non-genetic drivers of SLE: Implications of IRF5 dysregulation in both roads leading to SLE. *Curr. Rheumatol. Rep.* **21**, 2 (2019).
44. C. D. Thompson, B. Matta, B. J. Barnes, Therapeutic targeting of IRFs: Pathway-dependence or structure-based? *Front. Immunol.* **9**, 2622 (2018).
45. Y. Xu, P. Y. Lee, Y. Li, C. Liu, H. Zhuang, S. Han, D. C. Nacionales, J. Weinstein, C. E. Mathews, L. L. Moldawer, S. W. Li, M. Satoh, L. J. Yang, W. H. Reeves, Pleiotropic IFN-dependent and -independent effects of IRF5 on the pathogenesis of experimental lupus. *J. Immunol.* **188**, 4113–4121 (2012).
46. T. Krausgruber, D. Saliba, G. Ryzhakov, A. Lanfrancotti, K. Blazek, I. A. Udalova, IRF5 is required for late-phase TNF secretion by human dendritic cells. *Blood* **115**, 4421–4430 (2010).
47. W. E. Purtha, M. Swiecki, M. Colonna, M. S. Diamond, D. Battacharya, Spontaneous mutation of the Dock2 gene in *Irf5*$^{-/-}$ mice complicates interpretation of type I interferon production and antibody responses. *Proc. Natl. Acad. Sci. U.S.A.* **109**, E898–E904 (2012).
48. W. Chen, S. S. Lam, H. Srinath, Z. Jiang, J. J. Correia, C. A. Schiffer, K. A. Fitzgerald, K. Lin, W. E. Royer Jr., Insights into interferon regulatory factor activation from the crystal structure of dimeric IRF5. *Nat. Struct. Mol. Biol.* **15**, 1213–1220 (2008).
49. S. Schmidt, M. J. W. Adjobo-Hermans, R. Kohze, T. Enderle, R. Brock, F. Milletti, Identification of short hydrophobic cell-penetrating peptides for cytosolic peptide delivery by rational design. *Bioconjug. Chem.* **28**, 382–389 (2017).
50. J. DeMartino, N. Fotouhi, A. Hoffman, K-S. Huang, F. Milletti, S. Panicker, D. Srinivasan, S-L. Tan, Cell penetrating peptides which bind IRF5 (WO/2014/056813A1, 2014).
51. G. N. Zhao, D. S. Jiang, H. Li, Interferon regulatory factors: At the crossroads of immunity, metabolism, and disease. *Biochim. Biophys. Acta* **1852**, 365–378 (2015).
52. K. T. Chow, C. Wilkins, M. Narita, R. Green, M. Knoll, Y.-M. Loo, M. Gale Jr., Differential and overlapping immune programs regulated by IRF3 and IRF5 in plasmacytoid dendritic cells. *J. Immunol.* **201**, 3036–3050 (2018).
53. M. A. Doucey, L. Goffin, L. D. Naeher, O. Michielin, P. Baumgärtner, P. Guillaume, E. Palmer, I. F. Luescher, CD3 delta establishes a functional link between the T cell receptor and CD8. *J. Biol. Chem.* **278**, 3257–3264 (2003).
54. L. Bao, L. Ding, M. Yang, H. Ju, Noninvasive imaging of sialyltransferase activity in living cells by chemoselective recognition. *Sci. Rep.* **5**, 10947 (2015).
55. L. Ujlaky-Nagy, P. Nagy, J. Szollosi, G. Vereb, Flow cytometric FRET analysis of protein interactions. *Methods Mol. Biol.* **1678**, 393–419 (2018).
56. M. Hedl, J. Yan, C. Abraham, IRF5 and IRF5 disease-risk variants increase glycolysis and human M1 macrophage polarization by regulating proximal signaling and Akt2 activation. *Cell Rep.* **16**, 2442–2455 (2016).
57. M. Hedl, J. Yan, H. Witt, C. Abraham, IRF5 is required for bacterial clearance in human M1-polarized macrophages, and *IRF5* immune-mediated disease risk variants modulate this outcome. *J. Immunol.* **202**, 920–930 (2019).
58. H. M. Akilesh, M. B. Buechler, J. M. Duggan, W. O. Hahn, B. Matta, X. Sun, G. Gessay, E. Whalen, M. Mason, S. R. Presnell, K. B. Elkon, A. Lacy-Hulbert, B. J. Barnes, M. Pepper, J. A. Hamerman, Chronic TLR7 and TLR9 signaling drives anemia via differentiation of specialized hemophagocytes. *Science* **363**, eaao5213 (2019).
59. J. M. Guthridge, D. N. Clark, A. Templeton, N. Dominquez, R. Lu, G. S. Vidal, J. A. Kelly, K. M. Kauffman, J. B. Harley, P. M. Gaffney, J. A. James, B. D. Poole, Effects of IRF5 lupus risk haplotype on pathways predicted to influence B cell functions. *J. Biomed. Biotechnol.* **2012**, 594056 (2012)
60. F. Steinhagen, A. P. McFarland, L. G. Rodriquez, P. Tewary, A. Jarret, R. Savan, D. M. Klinman, IRF-5 and NF-kB p50 co-regulate IFN-β and IL-6 expression in TLR9-stimulated human plasmacytoid dendritic cells. *Eur. J. Immunol.* **43**, 1896–1906 (2013).
61. D. G. Saliba, A. Heger, H. L. Eames, S. Oikonomopoulos, A. Teixeira, K. Blazek, A. Androulidaki, D. Wong, F. G. Goh, M. Weiss, A. Byrne, M. Pasparakis, J. Ragoussis, I. A. Udalova, IRF5:RelA interaction targets inflammatory genes in macrophages. *Cell Rep.* **8**, 1308–1317 (2014).
62. M. Lopez-Pelaez, D. J. Lamont, M. Peggie, N. Shpiro, N. S. Gray, P. Cohen, Protein kinase IKKβ-catalyzed phosphorylation of IRF5 at Ser462 induces its dimerization and nuclear translocation in myeloid cells. *Proc. Natl. Acad. Sci. U.S.A.* **111**, 17432–17437 (2014).
63. J. Ren, X. Chen, Z. J. Chen, IKKbeta is an IRF5 kinase that instigates inflammation. *Proc. Natl. Acad. Sci. U.S.A.* **111**, 17438–17443 (2014).
64. J. Audie, C. Boyd, The synergistic use of computation, chemistry and biology to discover novel peptide-based drugs: The time is right. *Curr. Pharm. Des.* **16**, 567–582 (2010).
65. C. Bechara, S. Sagan, Cell-penetrating peptides: 20 years later, where do we stand? *FEBS Lett.* **587**, 1693–1702 (2013).
66. S. Oon, N. J. Wilson, I. Wicks, Targeted therapeutics in SLE: Emerging strategies to modulate the interferon pathway. *Clin. Transl. Immunol.* **5**, e79 (2016).
67. P. Dai, H. Cao, T. Merghoub, F. Avogadri, W. Wang, T. Parikh, C. M. Fang, P. M. Pitha, K. A. Fitzgerald, M. M. Rahman, G. McFadden, X. Hu, A. N. Houghton, S. Shuman, L. Deng, Myxoma virus induces type I interferon production in murine plasmacytoid dendritic cells via a TLR9/MyD88-, IRF5/IRF7-, and IFNAR-dependent pathway. *J. Virol.* **85**, 10814–10825 (2011).
68. M. E. Mancl, G. Hu, N. Sangster-Guity, S. L. Olshalsky, K. Hoops, P. Fitzgerald-Bocarsly, P. M. Pitha, K. Pinder, B. J. Barnes, Two discrete promoters regulate the alternatively spliced human interferon regulatory factor-5 isoforms. Multiple isoforms with distinct cell type-specific expression, localization, regulation, and function. *J. Biol. Chem.* **280**, 21078–21090 (2005).
69. A. Paun, J. T. Reinert, Z. Jiang, C. Medin, M. Y. Balkhi, K. A. Fitzgerald, P. M. Pitha, Functional characterization of murine interferon regulatory factor 5 (IRF-5) and its role in the innate antiviral response. *J. Biol. Chem.* **283**, 14295–14308 (2008).
70. D. Eisenberg, J. U. Bowie, R. Luthy, S. Choe, Three-dimensional profiles for analysing protein sequence-structure relationships. *Faraday Discuss.* 25–34 (1992).
71. G. Cruciani, M. Baroni, E. Carosati, M. Clementi, R. Valigi, S. Clementi, Peptide studies by means of principal properties of amino acids derived from MIF descriptors. *J. Chemom.* **18**, 146–155 (2004).

72. J. M. Steward, J. D. Young, *Solid Phase Peptide Synthesis* (Freemantle, 1968).
73. V. Trouplin, N. Boucherit, L. Gorvel, F. Conti, G. Mottola, E. Ghigo, Bone marrow-derived macrophage production. *J. Vis. Exp.* **81**, e50966 (2013).

Acknowledgments: We thank J. Wanner, D. Fry, A. Kuglslatter, and D. Mark for helpful suggestions and guidance. We thank C. Garvie for CD helicity data, S. Singh for suggestions using IDEAS software, and M. LaPan for help with data analysis. We thank D. Nannemann for helpful suggestions in scrambled peptide selection. **Funding:** This work was supported and funded by F. Hoffmann–La Roche, the Lupus Research Alliance (to B.J.B.), Department of Defense CDMRP Lupus Research Program W81XWH-18-1-0674 (to B.J.B.), NIH AR065959 (to B.J.B.), and EMD Serono Research and Development Institute Inc. **Author contributions:** D.S., F.M., D.R.B., C.W., S.-L.T., J.A.D., A.F.H., G.C., and B.J.B. planned and designed the experiments. J.B., D.S., D.L., C.-C.S., C.D.T., K.-S.H., S.S., S.H., B.M., M.L., Q.G., Y.G.Q., G.L., H.Q., M.D., J.Q., and L.L. performed the experiments and analyzed data. D.S., G.C., C.D.T., S-L.T., and B.J.B. analyzed experimental data. D.S., S-L.T., S.N., J.A.D., N.F., G.C., and B.J.B. prepared the manuscript. **Competing interests:** Disclosures: J.A.D., S.-L.T., and D.S. are inventors on patent application US20160009772A1 assigned to F. Hoffmann–La Roche AG. Application status abandoned as of 12 May 2019 as a matter of public record. Financial disclosures related to companies: G.C., C.-C.S., J.Q., M.D., and J.A.D. are employees of EMD Serono Research and Development Institute Inc. S.H. is employee of BMS. F.M. is the author of patent "Cell penetrating peptides & methods of identifying cell penetrating peptides" (WO2014001229A2) filed by F. Hoffmann–La Roche. J.A.D., N.F., A.F.H., K.-S.H., F.M., D.S., and S.-L.T. are authors of patent "Cell penetrating peptides which bind irf5" (US20160009772A1) filed by Hoffmann–La Roche Inc. **Data and materials availability:** All data needed to evaluate the conclusions in the paper are present in the paper and/or the Supplementary Materials. IRF5-CPPs may be available in limited quantity pending scientific review. Requests for IRF5-CPPs should be submitted to B.J.B. and G.C. Additional data related to this paper may be requested from the authors.

Submitted 20 May 2019
Accepted 5 March 2020
Published 15 May 2020
10.1126/sciadv.aay1057

Citation: J. Banga, D. Srinivasan, C.-C. Sun, C. D. Thompson, F. Milletti, K.-S. Huang, S. Hamilton, S. Song, A. F. Hoffman, Y. G. Qin, B. Matta, M. LaPan, Q. Guo, G. Lu, D. Li, H. Qian, D. R. Bolin, L. Liang, C. Wartchow, J. Qiu, M. Downing, S. Narula, N. Fotouhi, J. A. DeMartino, S.-L. Tan, G. Chen, B. J. Barnes, Inhibition of IRF5 cellular activity with cell-penetrating peptides that target homodimerization. *Sci. Adv.* **6**, eaay1057 (2020).